

A Deterministic Sampling Method via Maximum Mean Discrepancy Flow with Adaptive Kernel

Yindong Chen¹, Yiwei Wang², Chun Liu¹, and Lulu Kang^{*3}

¹Department of Applied Mathematics, Illinois Institute of Technology

²Department of Mathematics, University of California, Riverside

²Department of Mathematics and Statistics, University of Massachusetts, Amherst

Abstract

We propose a novel deterministic sampling method, EVI-MMD, to approximate a target distribution ρ^* by minimizing the kernel discrepancy, also known as the Maximum Mean Discrepancy (MMD). Leveraging the *energetic variational inference* framework (Wang et al., 2021), we transform the MMD minimization problem into solving a dynamic system of Ordinary Differential Equations (ODEs) for particles. The implicit Euler scheme is employed to solve the ODE system, leading to a proximal minimization problem at each iteration, which is efficiently addressed using optimization algorithms such as L-BFGS. A key innovation of our method is a dynamic bandwidth selection strategy for the Gaussian kernel, addressing a long-standing challenge in kernel-based methods. Comprehensive numerical experiments demonstrate that this adaptive bandwidth significantly enhances the performance of EVI-MMD. We apply the EVI-MMD algorithm to two types of sampling problems: (1) when the target distribution is fully specified by a density function, and (2) the “two-sample problem,” where only training data are available. In the latter case, EVI-MMD serves as a generative model, producing new samples that faithfully replicate the distribution of the training data. With carefully tuned parameters, EVI-MMD outperforms several existing methods in both scenarios.

Key words: Deterministic Sampling, Kernel Discrepancy, Generative Model, Maximum Mean Discrepancy (MMD), Proximal Minimization, Variational Inference.

1 Introduction

Many methods in statistics, machine learning, and applied mathematics require sampling from a certain target distribution. For example, in numerical integration, the multidimensional integration $I = \mathbb{E}_{\mathbf{x} \sim \mu}[f(\mathbf{X})] = \int_{\Omega} f(\mathbf{x})\mu(d\mathbf{x})$ is approximated by the sample mean $\hat{I}_n = \frac{1}{N} \sum_{i=1}^N f(\mathbf{x}_i)$, where the $f(\mathbf{x})$ is the integral function, μ is the probability measure with the support region Ω , and \mathbf{x}_i 's are the i.i.d. samples following the distribution of μ . Statistical design of experiments is also related to this area. One such instance is the uniform space-filling design (Fang et al., 2000), in which the design points should approximate the uniform distribution. Contrary to the two cases, where the target distribution is fully specified, in the “two-sample problem” the target distribution is completely unknown and only the training data are given. So the target distribution is the empirical distribution of the training data. Generative learning models can be used to generate new samples from the empirical distribution of training data in a parametric or nonparametric fashion. They

*Corresponding author: Lulu Kang (lulukang@umass.edu).

have gained a lot of attention and popularity due to the wide application of generative adversarial networks (or GANs) (Creswell et al., 2018; Goodfellow et al., 2014) and variational autoencoders (or VAE) (Kingma and Welling, 2013), which are built on parametric deep neural networks.

In recent decades, variational inference (VI) has become an important and popular tool in machine learning, statistics, applied mathematics (Jordan et al., 1999; Wibisono et al., 2016; David M. Blei and McAuliffe, 2017; Mnih and Rezende, 2016; Gorbach et al., 2017), etc. In short, the main goal of a VI method is to generate samples to approximate a target distribution. Naturally, VI is strongly tied to these aforementioned research areas. Its computational advantage has propelled the development of many VI-based supervised and unsupervised learning methods, such as Bayesian neural networks (Graves, 2011; Louizos and Welling, 2017; Wu et al., 2019; Shridhar et al., 2019), Gaussian process model (King and Lawrence, 2006; Nguyen and Bonilla, 2013, 2014; Sheth et al., 2015; Damianou et al., 2016; Chen et al., 2019a), and generative models (Kingma et al., 2014).

In this paper, we propose a new variational inference approach by minimizing the kernel discrepancy via the energetic variational approach (Wang et al., 2021). Essentially, we generate samples, or *particles*, to approximate various target distributions that are fully specified or empirically available from training data.

1.1 Related Works

The core idea of VI is to minimize a user-specified dissimilarity functional that measures the difference between two distributions. Many dissimilarity functionals, such as Kullback-Leibler (KL-)divergence and the more general f -divergence (Csiszár and Shields, 2004; Zhang et al., 2019), Wasserstein distance (Villani, 2021), kernel stein discrepancy (KSD) (Liu et al., 2016; Chen et al., 2018b), and kernel discrepancy, have been used in the literature.

If the target distribution is known up to the intractable normalizing constant, KL-divergence is commonly used (Liu and Wang, 2016; David M. Blei and McAuliffe, 2017; Ma et al., 2019; Heng et al., 2021). For example, the Langevin Monte Carlo (LMC) (Welling and Teh, 2011; Cheng et al., 2018; Bernton, 2018) and the Stein Variational Gradient Descent (SVGD) (Liu and Wang, 2016) can be considered as a discretization of the Wasserstein gradient flow (Jordan et al., 1998) of the KL-divergence. However, KL-divergence is only suitable for the target distribution whose density function takes the form $\frac{1}{Z} \exp(-V(\mathbf{x}))$. Moreover, the KL-divergence-based algorithms require repeated evaluation of the gradient of the target distribution, which can be computationally costly if the target distribution is complicated to compute.

Kernel discrepancy is another popular dissimilarity functional. In machine learning, kernel discrepancy is better known as *Maximum Mean Discrepancy* or *MMD*. It is suitable for the case where the target distribution is compactly supported. Unlike KL-divergence, MMD does not have the “log 0” issue which can occur when the density values are really small at certain particles. What is more, it is easy to compute the MMD for the two-sample problems (Li et al., 2015; Kingma et al., 2016a), in which the target distribution is the empirical distribution of training data. For these reasons, we choose kernel discrepancy or MMD as the objective functional. We defer the detailed review of kernel discrepancy/MMD and its related literature in Section 2.

Another important aspect of a VI approach is the minimization method. As reviewed by David M. Blei and McAuliffe (2017), the complexity of the minimization is largely decided by the distribution family \mathcal{Q} , i.e., the set of feasible distributions to approximate the target distribution. It can be a family of parametric distributions. But sometimes, the parametric distribution is too restrictive, and thus flow-based VI methods have been created, in which \mathcal{Q} consists of distributions obtained by a series of smooth transformations from a tractable initial reference distribution. Examples include normalizing flow VI methods (Rezende and Mohamed, 2015; Kingma et al., 2016b)

and particle-based VI methods (ParVIs) (Liu and Wang, 2016; Liu, 2017; Liu and Zhu, 2018; Chen et al., 2018a; Liu et al., 2019; Chen et al., 2019b; Wang et al., 2021; Arbel et al., 2019; Korba et al., 2021; Mroueh et al., 2019). Our proposed approach belongs to the ParVIs category. Among all the ParVIs, SVGD (Liu, 2017) is one of the most popular early works. We compare the proposed approach with some other ParVI methods, including SVGD.

1.2 Our Contributions

In this paper, we propose a deterministic sampling method by minimizing the kernel discrepancy or MMD via the general energetic variational inference (EVI) framework (Wang et al., 2021). The EVI transforms the minimization problem into a dynamic system, which can be solved by many numerical schemes, including the implicit Euler method as demonstrated in this paper. We name it *EVI-MMD* algorithm.

Compared to some existing works that also minimize MMD, the proposed approach applies to many scenarios, including the cases when the target distribution is fully known and empirically given by the data, whereas most existing MMD methods (Gretton et al., 2012; Li et al., 2015; Liu et al., 2016; Kingma et al., 2016a; Mak and Joseph, 2018; Chen et al., 2019c; Marius Hofert and Zhu, 2021) focus on the two-sample problem. Besides, the proposed EVI-MMD method is much simpler considering it does not need to construct any deep neural network as the flow map as in Arbel et al. (2019). The implicit Euler is stable because the MMD is guaranteed to be decreased in each iteration (Section 2.2). More importantly, we propose a novel way to specify the bandwidth dynamically. It overcomes a long-existing issue of bandwidth selection for the Gaussian kernel in many ParVI methods. Through a comprehensive numerical study, we show the proposed adaptive bandwidth significantly improves the EVI-MMD algorithm.

The rest of the paper is organized as follows. Section 2 gives the necessary background on the kernel discrepancy and the general deterministic sampling method by the EVI framework. In Section 3, we apply the general EVI framework to minimize the kernel discrepancy and discuss the practical issues of EVI-MMD, including the specification of adaptive bandwidth and other tuning parameters. In Section 4, three groups of examples are used to compare the EVI-MMD algorithm with some alternative methods. We conclude the paper in Section 5.

2 Background

We first review the concept of kernel discrepancy, which is better known as MMD in the machine learning literature, and then explain the EVI framework. The two combined are the foundation of the proposed EVI-MMD algorithm.

2.1 Kernel Discrepancy or MMD

Before its wide recognition in machine learning as MMD, kernel discrepancy has been an important concept in QMC literature and was promoted as a goodness-of-fit statistic and a quality measure for statistical experimental design (Hickernell, 1998, 1999; Fang et al., 2000; Fang and Mukerjee, 2000; Fang et al., 2002; Hickernell and Liu, 2002). Kernel discrepancy can be interpreted in different ways. Hickernell (2016) and Li et al. (2020) explained *three identities* of kernel discrepancy. First, it can be considered as a norm on a Hilbert space of measures, which has to include the Dirac measure. Second, it is commonly used as a deterministic cubature error bound for Monte Carlo methods. Third, it is the root mean squared cubature error, where the kernel function is also the

covariance function for a stochastic process. Here we review it using the second identity and then generalize it and connect it with MMD.

Let $\Omega \subset \mathbb{R}^d$ be the domain of a probability measure μ , which has density $\rho(\mathbf{x})$ and cumulative distribution function $F(\mathbf{x})$. The three concepts, measure, density, and CDF, are used interchangeably in the rest of the paper to refer to distribution. Let $(\mathcal{H}, \langle \cdot, \cdot \rangle_{\mathcal{H}})$ be a reproducing kernel Hilbert space (RKHS) of functions $f : \Omega \rightarrow \mathbb{R}$. By definition, the reproducing kernel, K , is the unique function defined on $\Omega \times \Omega$ with the properties that $K(\cdot, \mathbf{x}) \in \mathcal{H}$ for any $\mathbf{x} \in \Omega$ and $f(\mathbf{x}) = \langle K(\cdot, \mathbf{x}), f \rangle_{\mathcal{H}}$. The second property implies that K reproduces function values via the inner product. It can be verified that K is symmetric in its arguments and positive definite.

A cubature method approximates the integral $I = \int_{\Omega} f(\mathbf{x})\rho(\mathbf{x})d\mathbf{x} = \mathbb{E}_{\mathbf{x} \sim \mu}[f(\mathbf{X})]$ of an $f \in \mathcal{H}$ by the sample mean

$$\hat{I}_N = \frac{1}{N} \sum_{i=1}^N f(\mathbf{x}_i), \quad \text{where } \mathbf{x}_i \sim^{iid} F(\mathbf{x}).$$

Let $\mathcal{X} = \{\mathbf{x}_i\}_{i=1}^N$ be the set of the i.i.d. samples following $F(\mathbf{x})$ distribution. To measure the quality of the approximation, define the cubature error as

$$\text{err}(f, \mathcal{X}) = I - \hat{I}_N = \int_{\Omega} f(\mathbf{x})\rho(\mathbf{x})d\mathbf{x} - \frac{1}{N} \sum_{i=1}^N f(\mathbf{x}_i) = \int_{\Omega} f(\mathbf{x})d[F(\mathbf{x}) - F_{\mathcal{X}}(\mathbf{x})],$$

where $F_{\mathcal{X}}$ is the empirical CDF based on the sample \mathcal{X} . Under modest assumptions of the reproducing kernel, based on Cauchy-Schwarz inequality, the tight error bound is

$$|\text{err}(f, \mathcal{X})| \leq \|f\|_{\mathcal{H}} D(\mathcal{X}, F, K),$$

where $\|f\|_{\mathcal{H}}$ is the norm of the function f based on the inner product of the RKHS \mathcal{H} and $D(\mathcal{X}, F, K)$ is the kernel discrepancy whose square is equal to

$$\begin{aligned} D^2(\mathcal{X}, F, K) &= \int_{\Omega \times \Omega} K(\mathbf{x}, \mathbf{y})d[F(\mathbf{x}) - F_{\mathcal{X}}(\mathbf{x})]d[F(\mathbf{y}) - F_{\mathcal{X}}(\mathbf{y})] \\ &= \int_{\Omega \times \Omega} K(\mathbf{x}, \mathbf{y})dF(\mathbf{x})dF(\mathbf{y}) - \frac{2}{N} \sum_{i=1}^N \int_{\Omega} K(\mathbf{x}_i, \mathbf{y})dF(\mathbf{y}) + \frac{1}{N^2} \sum_{i,j=1}^N K(\mathbf{x}_i, \mathbf{x}_j). \end{aligned} \quad (1)$$

Recall that the kernel discrepancy is also the norm on a Hilbert space of measures, i.e., the first identity mentioned earlier. More specifically, this Hilbert space of measures, denoted by \mathcal{M} , is the closure of the pre-Hilbert space and its inner product is defined as

$$\langle \nu_1, \nu_2 \rangle_{\mathcal{M}} = \int_{\Omega \times \Omega} K(\mathbf{x}, \mathbf{y})\nu_1(d\mathbf{x})\nu_2(d\mathbf{y}).$$

For the given kernel K , the Hilbert space contains all measures such that $\|\nu\|_{\mathcal{M}}$ is bounded. Please see [Hickernell \(2016\)](#) or [Li et al. \(2020\)](#) for the detailed definitions of the RKHS \mathcal{H} , \mathcal{M} , and the derivation of (1). The kernel discrepancy can be more generally defined by

$$D^2(\nu_1, \nu_2, K) = \int_{\Omega \times \Omega} K(\mathbf{x}, \mathbf{y})[\nu_1(d\mathbf{x}) - \nu_2(d\mathbf{x})][\nu_1(d\mathbf{y}) - \nu_2(d\mathbf{y})], \quad (2)$$

measuring the difference between any $\nu_1, \nu_2 \in \mathcal{M}$. [Gretton et al. \(2012\)](#) defined the maximum mean discrepancy (MMD) as

$$\text{MMD}(\mathcal{H}, \nu_1, \nu_2) = \sup_{f \in \mathcal{H}} (\mathbb{E}_{\mathbf{x} \sim \nu_1}[f(\mathbf{x})] - \mathbb{E}_{\mathbf{y} \sim \nu_2}[f(\mathbf{y})]),$$

and under the same definition of \mathcal{H} and \mathcal{M} , the square of MMD is

$$\text{MMD}^2(\mathcal{H}, \nu_1, \nu_2) = \mathbb{E}_{\mathbf{x}, \mathbf{x}' \sim \nu_1} [K(\mathbf{x}, \mathbf{x}')] - 2\mathbb{E}_{\mathbf{x} \sim \nu_1, \mathbf{y} \sim \nu_2} [K(\mathbf{x}, \mathbf{y})] + \mathbb{E}_{\mathbf{y} \sim \nu_2, \mathbf{y}' \sim \nu_2} [K(\mathbf{y}, \mathbf{y}')],$$

which is equivalent to $D^2(\nu_1, \nu_2, K)$ in (2). Therefore, in the rest of the paper, we use kernel discrepancy and MMD interchangeably.

Kernel discrepancy has many desirable properties, one of which is measuring the difference between distributions. In fact, $\text{MMD}(\mathcal{H}, \nu_1, \nu_2) = 0$ if and only if $\nu_1 = \nu_2$, provided that Ω is a compact metric space and more importantly, K is a universal kernel and thus \mathcal{H} is a universal RKHS (Gretton et al., 2012). Simply put, universal kernel (Micchelli et al., 2006) means that K has to be complex enough such that \mathcal{H} and \mathcal{M} are sufficiently big. Lower-order polynomial kernels, such as linear and second-order polynomials are not universal. MMD induced by the second-order polynomial kernel can distinguish two distributions in terms of mean and variance, and the linear kernel can only do so in terms of the mean. On the other hand, the Gaussian kernel is universal and thus the MMD based on it can be used as a metric for measures (Micchelli et al., 2006; Fukumizu et al., 2007). Therefore, with a proper kernel, if $D^2(\mathcal{X}_N, F, K) \rightarrow 0$ as $N \rightarrow \infty$, then $F_{\mathcal{X}_N} \rightarrow F$. For fixed N , if $D^2(\mathcal{X}, F, K) \rightarrow 0$ as $n \rightarrow \infty$ (n is the notation for iteration of algorithm), then $F_{\mathcal{X}} \rightarrow F$. Kernel discrepancy is also related to energy distance (Székely and Rizzo, 2013) and support points (Mak and Joseph, 2018). If set $K(\mathbf{x}, \mathbf{y}) = -\|\mathbf{x} - \mathbf{y}\|_2^2$, then the kernel discrepancy becomes energy distance. For the two-sample problem, the energy distance is given by

$$E(F_n, F) = \frac{2}{N \cdot M} \sum_{i=1}^N \sum_{l=1}^M \|\mathbf{x}_i - \mathbf{y}_l\|_2 - \frac{1}{N^2} \sum_{i,j} \|\mathbf{x}_i - \mathbf{x}_j\|_2 - \frac{1}{M^2} \sum_{l,k=1}^M \|\mathbf{y}_l - \mathbf{y}_k\|_2. \quad (3)$$

2.2 Deterministic Sampling through EVI

Motivated by the energetic variational approaches for modeling the dynamics of non-equilibrium thermodynamical systems (Giga et al., 2017), the energetic variational inference (EVI) framework uses a continuous energy-dissipation law to specify the dynamics of minimizing the objective function in machine learning problems. Under the EVI framework, a practical algorithm can be obtained by introducing a suitable discretization to the continuous energy-dissipation law. This idea was introduced and applied to variational inference by Wang et al. (2021). It can also be applied to other machine learning problems similar to Trillos and Sanz-Alonso (2020) and E et al. (2020).

We first introduce the EVI using the continuous formulation. Let ϕ_t be the dynamic flow map $\phi_t : \mathbb{R}^d \rightarrow \mathbb{R}^d$ that continuously transforms the d -dimensional distribution from an initial distribution toward the target one and we require the map ϕ_t to be smooth and one-to-one. Let $\rho_{[\phi_t]}$ denote the probability density that is transformed by ϕ_t from an initial distribution. For a given target distribution ρ^* , one can define a functional $\mathcal{F}(\phi_t) = D(\rho_{[\phi_t]} || \rho^*)$, where D is the user-specified dissimilarity functional, such as the KL-divergence in Wang et al. (2021). Taking the analogy of a thermodynamics system, $\mathcal{F}(\phi_t)$ can be viewed as the Helmholtz free energy. Following the First and Second Law of thermodynamics (Giga et al., 2017) (kinetic energy is set to be zero), one can impose the following energy-dissipation

$$\frac{d}{dt} \mathcal{F}(\phi_t) = -\Delta(\phi_t, \dot{\phi}_t), \quad (4)$$

to describe a dynamics of minimizing $\mathcal{F}(\phi_t)$. Here $\Delta(\phi_t, \dot{\phi}_t)$ is a user-specified functional representing the rate of energy dissipation, and $\dot{\phi}_t$ is the derivative of ϕ_t with time t . So $\dot{\phi}_t$ can be interpreted as the “velocity” of the transformation. Each variational formulation gives a natural

path of decreasing the objective functional $\mathcal{F}(\phi_t)$ toward an equilibrium (Trillos and Sanz-Alonso, 2020).

The dissipation functional should satisfy $\Delta(\phi_t, \dot{\phi}_t) \geq 0$ so that $\mathcal{F}(\phi_t)$ decreases with time. As discussed in Wang et al. (2021), there are many ways to specify $\Delta(\phi_t, \dot{\phi}_t)$ and the simplest among them is a quadratic functional in terms of $\dot{\phi}_t$,

$$\Delta(\phi_t, \dot{\phi}_t) = \int_{\Omega_t} \eta(\rho_{[\phi_t]}) \|\dot{\phi}_t\|_2^2 d\mathbf{x}, \quad (5)$$

where $\rho_{[\phi_t]}$ denotes the pdf of the current distribution which is the initial distribution transformed by ϕ_t , $\eta(\cdot)$ is a user-specified positive function of $\rho_{[\phi_t]}$, Ω_t is the current support, and $\|\mathbf{a}\|_2 = \sqrt{\mathbf{a}^\top \mathbf{a}}$ for $\forall \mathbf{a} \in \mathbb{R}^d$.

With the specified energy-dissipation law (4), the energy variational approach derives the dynamics of the systems through two variational procedures, the Least Action Principle (LAP) and the Maximum Dissipation Principle (MDP), which leads to

$$\frac{\delta \frac{1}{2} \Delta}{\delta \dot{\phi}_t} = -\frac{\delta \mathcal{F}}{\delta \phi_t}.$$

The approach is motivated by the seminal works of Raleigh (Rayleigh, 1873) and Onsager (Onsager, 1931a,b). Using the quadratic $\Delta(\phi_t, \dot{\phi}_t)$ (5), the dynamics of decreasing \mathcal{F} is

$$\eta(\rho_{[\phi_t]}) \dot{\phi}_t = -\frac{\delta \mathcal{F}}{\delta \phi_t}. \quad (6)$$

In general, this continuous formulation is difficult to solve, since the manifold of ϕ_t is of infinite dimension. Naturally, there are different approaches to approximating an infinite-dimensional manifold by a finite-dimensional manifold. One such approach, as used in Wang et al. (2021), is to use particles (or samples) to approximate the continuous distribution $\rho_{[\phi_t]}$ with kernel regularization. If this approximation applies to (6), after the LAP and MDP variational steps, we call it the “variation-then-approximation” approach. If this approximation is applied to (4) directly, before any variational steps, we call it the “approximation-then-variation” approach. The latter leads to a discrete version of the energy-dissipation law, i.e.,

$$\frac{d}{dt} \mathcal{F}_h(\{\mathbf{x}_i(t)\}_{i=1}^N) = -\Delta_h(\{\mathbf{x}_i(t)\}_{i=1}^N, \{\dot{\mathbf{x}}_i(t)\}_{i=1}^N). \quad (7)$$

Here $\{\mathbf{x}_i(t)\}_{i=1}^N$ are the locations of N particles at time t and $\dot{\mathbf{x}}_i(t)$ is the derivative of \mathbf{x}_i with t , and thus is the velocity of the i th particle as it moves toward the target distribution. The functional \mathcal{F}_h and Δ_h are the discretized free energy and dissipation by the N particles. The subscript h of \mathcal{F}_h and Δ_h denotes the bandwidth parameter of the kernel function used in the kernelization operation. Applying the variational steps to (7), we obtain the dynamics of decreasing \mathcal{F} at the particle level,

$$\frac{\delta \frac{1}{2} \Delta_h}{\delta \dot{\mathbf{x}}_i(t)} = -\frac{\delta \mathcal{F}_h}{\delta \mathbf{x}_i}, \quad \text{for } i = 1, \dots, N. \quad (8)$$

This leads to an ODE system of $\{\mathbf{x}_i(t)\}_{i=1}^N$ that can be solved by different numerical schemes. The solution of the ODE system is the particles approximating the target distribution. Using the dissipation $\Delta(\phi_t, \dot{\phi}_t) = G \int_{\Omega_t} \rho_{[\phi_t]} \|\dot{\phi}_t\|_2^2 d\mathbf{x}$, the discretized dissipation is $\Delta_h = -\frac{G}{N} \sum_{i=1}^N \|\dot{\mathbf{x}}_i(t)\|_2^2$, where G is a positive constant. Then (8) becomes

$$\frac{G}{N} \dot{\mathbf{x}}_i = -\frac{\delta \mathcal{F}}{\delta \mathbf{x}_i}(\{\mathbf{x}_i\}_{i=1}^N), \quad \text{for } i = 1, \dots, N. \quad (9)$$

The most straightforward way to solve (8) is the explicit Euler method, which is equivalent to minimizing \mathcal{F}_h using the gradient descent method. Another approach is to adopt the implicit Euler scheme to solve the ODE system. This is done by discretizing the left-hand side of (8) in time t and replacing the $\{\mathbf{x}_i\}_{i=1}^N$ by $\{\mathbf{x}_i^{n+1}\}_{i=1}^N$ for $i = 1, \dots, N$ in the right-hand side, i.e.,

$$\frac{G}{N} \frac{\mathbf{x}_i^{(n+1)} - \mathbf{x}_i^{(n)}}{\tau} = -\frac{\delta \mathcal{F}}{\delta \mathbf{x}_i}(\{\mathbf{x}_i^{n+1}\}_{i=1}^N). \quad (10)$$

Note that if $\{\mathbf{x}_i\}_{i=1}^N$ is replaced by $\{\mathbf{x}_i^n\}_{i=1}^N$ in the right-hand side, it leads to the explicit Euler scheme. It is easy to show that a solution of the nonlinear system (10) can be obtained by solving an optimization problem

$$\{\mathbf{x}_i^{(n+1)}\}_{i=1}^N = \arg \min_{\{\mathbf{x}_i\}_{i=1}^N} (J_n(\{\mathbf{x}_i\}_{i=1}^N)),$$

where

$$J_n(\{\mathbf{x}_i\}_{i=1}^N) := \frac{G}{2\tau N} \sum_{i=1}^N \|\mathbf{x}_i - \mathbf{x}_i^{(n)}\|_2^2 + \mathcal{F}_h(\{\mathbf{x}_i\}_{i=1}^N). \quad (11)$$

We can therefore define the general EVI Algorithm 1. It shares some resemblance in structure with the proximal point algorithm (Rockafellar, 1976). Compared to the explicit Euler method, the implicit method is more stable even with a relatively large step size τ . Indeed, it can be shown that (Wang et al., 2021)

$$\mathcal{F}_h(\{\mathbf{x}_i^{n+1}\}) \leq J_n(\{\mathbf{x}_i^{n+1}\}_{i=1}^N) \leq J_n(\{\mathbf{x}_i^n\}_{i=1}^N) = \mathcal{F}(\{\mathbf{x}_i^n\}).$$

So the set of particles always reduces $\mathcal{F}_h(\{\mathbf{x}_i\}_{i=1}^N)$ in each iteration. Many other novel approaches can be proposed by applying different numerical algorithms to solve (8) and/or by transforming the original optimization problem into a differential equation system.

Algorithm 1 The Implicit EVI Algorithm

Require: ρ_0 : the distribution of the initial particles

N : total number of particles

maxIter: the total number of iterations

τ : step size of implicit Euler

G : user-specified positive constant for proper scaling

h : bandwidth parameter of the kernel function

1: Generate initial particles $\{\mathbf{x}_i^0\}_{i=1}^N$ from a distribution ρ_0 .

2: **for** $n = 0 : \text{maxIter}$ **do**

3: $\{\mathbf{x}_i^{(n+1)}\}_{i=1}^N = \arg \max_{\{\mathbf{x}_i\}^N} \frac{G}{2\tau N} \sum_{i=1}^N \|\mathbf{x}_i^{(n)} - \mathbf{x}_i\|_2^2 + \mathcal{F}_h(\{\mathbf{x}_i\}_{i=1}^N)$

4: **end for**

3 Practical EVI-MMD Algorithm

Given the target probability measure μ whose CDF is F , and the proper reproducing kernel K , we choose the squared kernel discrepancy $D^2(\mathcal{X}_N, F, K)$ as the discrete free energy \mathcal{F}_h , i.e.,

$$\mathcal{F}_h(\{\mathbf{x}_i(t)\}_{i=1}^N) = D^2(\{\mathbf{x}_i(t)\}_{i=1}^N, F, K), \quad (12)$$

which measures the difference between the empirical distribution of the particles and the target distribution. We call Algorithm 1 with (12) as the *EVI-MMD* algorithm. To make sure the EVI-MMD performs well in general, there are still some challenges. In this section, we address each challenge and propose a practical EVI-MMD algorithm.

3.1 Estimation of the Free Energy

The first challenge is how to estimate the free energy $D^2(\{\mathbf{x}_i(t)\}_{i=1}^N, F, K)$ efficiently. There are three terms in $D^2(\{\mathbf{x}_i(t)\}_{i=1}^N, F, K)$ in (1). The first term $\int_{\Omega \times \Omega} K(\mathbf{x}, \mathbf{y}) dF(\mathbf{x}) dF(\mathbf{y})$ only depends on the target distribution and does not affect the minimization with respect to the particles. So we do not need to compute it in the optimization procedure. The third term $\frac{1}{N^2} \sum_{i,j=1}^N K(\mathbf{x}_i, \mathbf{x}_j)$ is easily calculated based on the particles $\{\mathbf{x}_i(t)\}_{i=1}^N$, which we call “square-term”. Assume $\rho^*(\mathbf{y})$ is the probability density function associated with the target CDF $F(\mathbf{x})$. The main challenge is how to compute the “cross-term” in (1), i.e.,

$$\sum_{i=1}^N \int_{\Omega} K(\mathbf{x}_i, \mathbf{y}) dF(\mathbf{y}) = \sum_{i=1}^N \int_{\Omega} K(\mathbf{x}_i, \mathbf{y}) \rho^*(\mathbf{y}) d\mathbf{y}. \quad (13)$$

Since it is difficult to sample from $\rho^*(\mathbf{y})$ directly, one cannot use any standard Monte Carlo integration. Fortunately, using the Gaussian kernel $K(\mathbf{x}_i, \mathbf{x}_j) = \exp\left(-\frac{\|\mathbf{x}_i - \mathbf{x}_j\|_2^2}{2h^2}\right)$, one can estimate this integration by generating samples from a Gaussian distribution. Indeed, for the Gaussian kernel, the cross-term can be estimated by

$$\sum_{i=1}^N \int_{\Omega} \exp\left(-\frac{\|\mathbf{y} - \mathbf{x}_i\|_2^2}{2h^2}\right) \rho^*(\mathbf{y}) d\mathbf{y} = \sum_{i=1}^N C_h \mathbb{E}_{\mathbf{y} \sim \mathcal{N}(\mathbf{x}_i, h^2 \mathbf{I}_d)}[\rho^*(\mathbf{y})] \approx \sum_{i=1}^N \frac{C_h}{L} \sum_{l=1}^L \rho^*(\mathbf{x}_i + h\boldsymbol{\xi}_l), \quad (14)$$

where $\{\boldsymbol{\xi}_l\}_{l=1}^L$ are sampled from the d -dimensional standard normal $\mathcal{N}(\mathbf{0}, \mathbf{I}_d)$ and $C_h = (2\pi)^{d/2} h^d$ is the normalizing constant. The gradient of the cross-term with respect to \mathbf{x}_i is also easy to compute based on the approximation (14), i.e.,

$$\nabla_{\mathbf{x}_i} \left(\sum_{i=1}^N \int_{\Omega} \exp\left(-\frac{\|\mathbf{y} - \mathbf{x}_i\|_2^2}{2h^2}\right) \rho^*(\mathbf{y}) d\mathbf{y} \right) \approx \sum_{i=1}^N \frac{C_h}{L} \sum_{l=1}^L \nabla_{\mathbf{x}_i} \rho^*(\mathbf{x}_i + h\boldsymbol{\xi}_l). \quad (15)$$

Other than the Gaussian kernel, any other positive kernel function that is proportional to a certain density function and easy to be sampled from can be used here. In this paper, we use the Gaussian kernel when the target distribution is fully specified. Theoretically, it is unclear if the error in estimating the cross-term will significantly affect the final performance of EVI-MMD. In the numerical examples in Section 4 we set $L = 100$ or 500 depending on the scale of the problem and the computational cost. It is shown to achieve a good numerical performance.

If the target distribution is an empirical one and only available from the training data $\{\mathbf{y}_i\}_{i=1}^M$ with sample size M , i.e., the two-sample problem, it is easy to estimate the cross-term by

$$\sum_{i=1}^N \int_{\Omega} K(\mathbf{x}_i, \mathbf{y}) dF(\mathbf{y}) = \frac{1}{M} \sum_{i=1}^N \sum_{j=1}^M K(\mathbf{x}_i, \mathbf{y}_j). \quad (16)$$

Due to the fact that $F(\mathbf{y})$ represents the empirical CDF of the training data, the numerical integration is exactly as in (16) and no approximation is involved. To reduce computation for large

data, we can use the mini-batch procedure, which means randomly drawing a subset of samples $\{\mathbf{y}_i\}_{i=1}^L$ from $\{\mathbf{y}_i\}_{i=1}^M$ to compute (16) in each iteration. For the two-sample problem, we can use kernels other than the Gaussian kernel. In Section 4, we also use the kernel $K(\mathbf{x}, \mathbf{y}) = -\|\mathbf{x} - \mathbf{y}\|_2$ which leads to the energy distance and compare it with the Gaussian kernel using the EVI-MMD algorithm.

3.2 Choice of the Ratio G/τ

The parameter τ is interpreted as the time step size in the implicit Euler in (10). The positive constant G is to scale the dissipation law to suit the chosen free energy. It is easy to see from Algorithm 1 that only the ratio $\tau^* = \tau/G$ affects the implicit Euler procedure, so we consider how to choose τ^* . Notice that

$$\begin{aligned} J_n(\{\mathbf{x}_i^{(n+1)}\}_{i=1}^N) &= \frac{1}{2\tau^*N} \sum_{i=1}^N \|\mathbf{x}_i^{(n+1)} - \mathbf{x}_i^{(n)}\|_2^2 + \mathcal{F}_h(\{\mathbf{x}_i^{(n+1)}\}_{i=1}^N) \\ &\leq J_n(\{\mathbf{x}_i^{(n)}\}_{i=1}^N) = \mathcal{F}_h(\{\mathbf{x}_i^{(n)}\}_{i=1}^N), \end{aligned}$$

which indicates

$$\sum_{i=1}^N \|\mathbf{x}_i^{(n+1)} - \mathbf{x}_i^{(n)}\|_2^2 \leq 2\tau^*N |\mathcal{F}_h(\{\mathbf{x}_i^{(n)}\}_{i=1}^N) - \mathcal{F}_h(\{\mathbf{x}_i^{(n+1)}\}_{i=1}^N)|. \quad (17)$$

The above inequality shows that, in each iteration, the displacement of the particles, i.e., the left-hand side of the inequality, is bounded above by the change of \mathcal{F}_h . For Gaussian kernel, the scale of $|\mathcal{F}_h(\{\mathbf{x}_i^{(n)}\}_{i=1}^N) - \mathcal{F}_h(\{\mathbf{x}_i^{(n+1)}\}_{i=1}^N)|$ is almost independent with the dimension. As a result, the convergence of the algorithm can be extremely slow for high-dimensional problems because $\sum_{i=1}^N \|\mathbf{x}_i^{(n+1)} - \mathbf{x}_i^{(n)}\|_2^2$ can be small if τ^* is small. This observation motivates us to pick a relatively large τ^* to balance the scale of the first and second terms in $J_n(\{\mathbf{x}_i^{(n+1)}\}_{i=1}^N)$. We have done extensive numerical experiments and they suggest taking $\tau^* \approx d$, which is the dimension of \mathbf{x} . More detailed discussions on tuning parameters are in Section 3.4.

3.3 Adaptive Bandwidth Selection for Gaussian Kernel

Kernel selection is an important component in any MMD-based algorithm. The key question is how to choose the bandwidth since it is much easier to select the proper kernel function based on the problem. Bandwidth parameter significantly affects the efficiency and robustness of the algorithm (Briol et al., 2019). Although some approaches have been proposed in the literature (Bińkowski et al., 2021; Briol et al., 2019; Kingma et al., 2016a), a satisfactory and universal solution is still not achieved yet.

In this paper, we propose a new adaptive bandwidth selection for the Gaussian kernel $K(\mathbf{x}, \mathbf{y}) = \exp(-\|\mathbf{x} - \mathbf{y}\|^2/2h^2)$. We have done extensive numerical studies and observed the following trend. If the bandwidth h is too small, there will be outliers that converge too slowly toward the target distribution, whereas if h is too large, all the particles will eventually collapse to the same location as the algorithm iterates.

To illustrate this point, we construct a toy example to demonstrate different patterns of the decreasing MMD² curves with different bandwidth settings. For a given $\theta \in [0, 2]$, we generate samples $\{\mathbf{x}_i^\theta\}_{i=1}^N$ from the model $\mathbf{x}_i^\theta = \mathbf{y}_i + (2 - \theta)\mathbf{z}_i$, where \mathbf{z}_i is sampled from a two-dimensional standard Gaussian distribution and \mathbf{y}_i is sampled from the fully specified target distribution, an

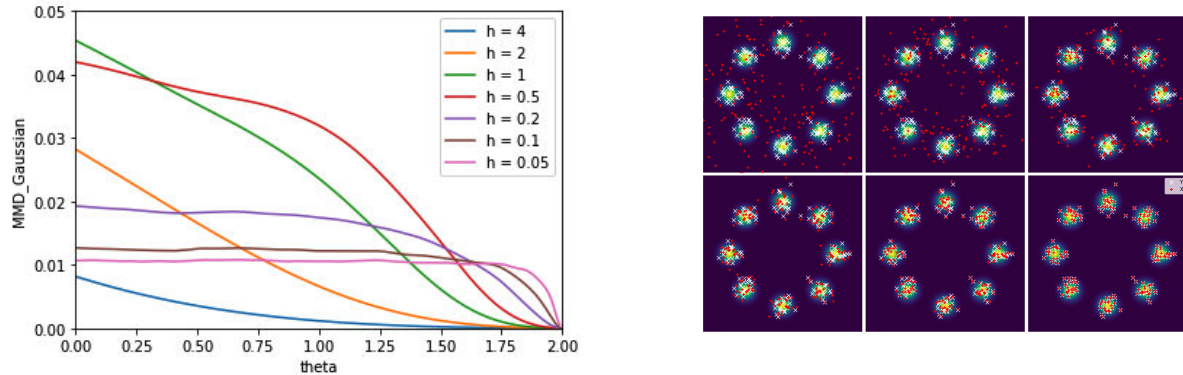


Figure 1: Left: decreasing MMD^2 curves with respect to $\theta \in [0, 2]$ using different h . Right: from the first to the second row and from left to right, for $\theta = 0, 1, 1.5, 1.75, 1.9, 2$, the red dots are samples $\{\mathbf{x}_i^\theta\}_{i=1}^N$ and are plotted on the contour plot of the target distribution.

eight-component Gaussian mixture distribution (the second toy example in Section 4.1). It is obvious that as $\theta \rightarrow 2$, $\{\mathbf{x}_i^\theta\}_{i=1}^N$ converges to the target distribution. Indeed, in the right panel of Figure 1, the samples $\{\mathbf{x}_i^\theta\}_{i=1}^N$ (red dots) are closer to the Gaussian mixture distribution (green contour plot) as $\theta \rightarrow 2$. Using the Gaussian kernel, we compute $\text{MMD}^2(\{\mathbf{x}_i^\theta\}_{i=1}^N, \{\mathbf{y}_i\}_{i=1}^N)$ for different θ and h values. It is expected that all MMD^2 curves decrease to zero as $\theta \rightarrow 2$ as shown in the left panel of Figure 1. But they have very different decreasing patterns. For $h = 0.5, 1, 2, 4$, the MMD^2 decreases very fast initially when θ is small but much slower when θ is close to 2. For $h = 0.05, 0.1, 0.2$, the trend of MMD^2 is completely opposite. The curves are flat initially for θ in the range of $(0, 1.75)$ and drop to zero very fast near the end.

In this toy example, samples $\{\mathbf{x}_i^\theta\}_{i=1}^N$ of different θ values mimic the particles that are evolving toward the target distribution in the EVI-MMD algorithm. Generalizing this observation to any MMD-based algorithm, the convergence of the particles is not at the optimal speed if h is fixed throughout the algorithmic iteration. Therefore, we should choose a relatively large h at the beginning of the iteration and gradually decrease h . In this way, we can take advantage of the fast descent of MMD^2 both at the early and end stages of the algorithm and avoid the plateau. The idea behind such an operation is “exploration v.s. exploitation”. In the early stage, with a large h , the particles would explore a large neighborhood to find the region with a higher density of the target distribution. As the algorithm proceeds, when most particles are already at the region with a high probability density, the particles only need to exploit their close neighborhood and adjust their positions relative to other particles. As a result, the particles appear to align more regularly as shown in the toy examples in Section 4.1

Based on this idea, we propose to specify the bandwidth as follows,

$$h_n = \frac{a}{n^c} + b, \quad (18)$$

where n is the iteration index and a , b , and c are three user-specified parameters. Among them, $a = h_0 - b$ and we set it to be the median of the pairwise distance between the initial particles. In our examples, the initial distribution is a uniform distribution with a proper domain. The domain is obtained from the fully specified target distribution or from the training data in two-sample problems. The parameter $b > 0$ is a regulatory parameter, which serves as a lower bound of h_n . It is not very influential to the algorithm since it is only to stop h_n from becoming zero. For

lower-dimensional problems, such as the examples in Section 4.1 and 4.2, we set $b = 0.01$. For high-dimensional problems, such as the image data in Section 4.3, we set $b = 1$. In fact, in all our examples, when $n = \text{maxIter}$ (in Algorithm 2), h_n is still significantly larger than b , and the largest maxIter we have used is 5000 (in this case a is also very large). The parameter $c > 0$ decides the rate of decrease of the bandwidth with respect to n . More discussion about the tuning parameters is in Section 3.4

3.4 EVI-MMD with Adaptive Bandwidth

We summarize the EIV-MMD method using the Gaussian kernel and the adaptive bandwidth selection in Algorithm 2. For the problem with a fully specified target distribution, the free energy is

$$\begin{aligned} \mathcal{F}_{h_n}^* (\{\mathbf{x}_i\}_{i=1}^N) &= \int_{\Omega \times \Omega} \exp\left(-\frac{\|\mathbf{x} - \mathbf{y}\|_2^2}{2h_n^2}\right) \rho^*(\mathbf{x})\rho^*(\mathbf{y})d\mathbf{x}d\mathbf{y} - \frac{2}{N} \frac{C_{h_n}}{L} \sum_{i=1}^N \sum_{l=1}^L \rho^*(\mathbf{x}_i + h_n \boldsymbol{\xi}_l) \\ &+ \frac{1}{N^2} \sum_{i,j=1}^N \exp\left(-\frac{\|\mathbf{x}_i - \mathbf{x}_j\|_2^2}{2h_n^2}\right). \end{aligned}$$

For the two-sample problem (training data size is M), the free energy is

$$\begin{aligned} \mathcal{F}_{h_n}^* (\{\mathbf{x}_i\}_{i=1}^N) &= \frac{1}{M^2} \sum_{l,k=1}^M \exp\left(-\frac{\|\mathbf{y}_l - \mathbf{y}_k\|_2^2}{2h_n^2}\right) - \frac{2}{N \cdot M} \sum_{i=1}^N \sum_{j=1}^M \exp\left(-\frac{\|\mathbf{x}_i - \mathbf{y}_j\|_2^2}{2h_n^2}\right) \\ &+ \frac{1}{N^2} \sum_{i,j=1}^N \exp\left(-\frac{\|\mathbf{x}_i - \mathbf{x}_j\|_2^2}{2h_n^2}\right). \end{aligned}$$

The constant term (first term) in the free energy is not relevant to the optimization with respect to the particles and thus they are not computed in the optimization. For the large two-sample problems, the cross term and square term (the second and third term) are computed using the mini-batch procedure to save computation. There are many methods available to solve the proximal point minimization in each iteration. We have chosen the L-BFGS method (Liu and Nocedal, 1989) and it performs adequately.

In the Supplement, we use the eight-component Gaussian mixture as the target distribution and show the performance of Algorithm 2. Different combination of a , c , and τ^* are used. From this example and many other simulation studies we have done, we recommend the following settings for all the tuning parameters.

- $\tau^* \approx d$
- a is the median of all the pairwise distances between the initial particles.
- b is 0.01 or 1 depending on the dimension of the problem.
- c is mostly selected by trial-and-error and the usual candidates we have tried are $c = 0.2, 0.5$.
- L is set based on the dimension of the problem as well as the constraint of the computation cost. In general, a bigger L value leads to more accurate estimations of the free energy and its derivative.
- maxIter should be large enough to ensure the convergence of MMD^2 and the particles.

Algorithm 2 The EVI-MMD Algorithm with Adaptive Bandwidth

Require: ρ_0 : initial distribution of the particles. By default, we use the uniform distribution with a proper domain.

τ^* : we set $\tau^* = d$, the dimension of the problem

N : total number of particles

L : the size of samples to generate $\boldsymbol{\xi}_l \sim \mathcal{N}(\mathbf{0}, \mathbf{I}_d)$ for $l = 1, \dots, L$ or the size of the mini-batch

maxIter: the maximum number of iterations

b, c : parameters for vanishing bandwidth for the Gaussian kernel

1: Generate initial particles $\{\mathbf{x}_i^{(1)}\}_{i=1}^N$ from a distribution ρ_0 .

2: $a = \text{median}\{\|\mathbf{x}_i - \mathbf{x}_j\|, i, j = 1, \dots, N\}$.

3: Generate i.i.d. samples $\boldsymbol{\xi}_l \sim \mathcal{N}(\mathbf{0}, \mathbf{I}_d)$ for $l = 1, \dots, L$.

4: **for** $n = 1 : \text{maxIter}$ **do**

5: $h_n = a/n^c + b$

6: $\{\mathbf{x}_i^{(n+1)}\}_{i=1}^N = \arg \max_{\{\mathbf{x}_i\}^N} \frac{1}{2\tau^*N} \sum_{i=1}^N \|\mathbf{x}_i^{(n)} - \mathbf{x}_i\|^2 + \mathcal{F}_{h_n}^*(\{\mathbf{x}_i\}_{i=1}^N)$

7: **end for**

- N is largely based on consideration of the computational cost.

Although we recommend these rules-of-thumb on the tuning parameters, users should still run multiple trials to select the best possible combination of the tuning parameters for their problems in practice.

4 Numerical Examples

In this section, we demonstrate the performance of the proposed EVI-MMD algorithm through three types of examples. They cover two scenarios in which the target distribution is fully specified and the two-sample problems. In the latter case, the EVI-MMD is an effective generative model.

In all examples, we set a as the median of the pairwise distance of the initial particles and $\tau^* = d$. We set $b = 0.01$ for the examples in Section 4.1 and 4.2 and $b = 1$ in Section 4.3. For the parameter c , through trial-and-error, we set $c = 0.5$ for the examples in Section 4.1, $c = 0.1$ in Section 4.2 and $c = 0.2$ in Section 4.3. All algorithms and examples are implemented in Pytorch 1.10.1 (Paszke et al., 2019). The computation was performed on the Open Science Grid (Pordes et al., 2007; Sfiligoi et al., 2009).

4.1 Toy Examples

We test the Algorithm 2 in three toy examples where the target distributions are listed below.

1. Star-shaped five-component Gaussian mixture distribution:

$$\rho(\mathbf{x}) = \frac{1}{5} \sum_{i=1}^5 N(\mathbf{x}|\boldsymbol{\mu}_i, \boldsymbol{\Sigma}_i),$$

where for $i = 1, \dots, 5$,

$$\boldsymbol{\mu}_i = \begin{bmatrix} \cos\left(\frac{2\pi}{5}\right), & -\sin\left(\frac{2\pi}{5}\right) \\ \sin\left(\frac{2\pi}{5}\right), & \cos\left(\frac{2\pi}{5}\right) \end{bmatrix}^{i-1} \begin{bmatrix} 1.5 \\ 0 \end{bmatrix}, \quad \boldsymbol{\Sigma}_i = \begin{bmatrix} \cos\left(\frac{2\pi}{5}\right), & -\sin\left(\frac{2\pi}{5}\right) \\ \sin\left(\frac{2\pi}{5}\right), & \cos\left(\frac{2\pi}{5}\right) \end{bmatrix}^{i-1} \begin{bmatrix} 1, & 0 \\ 0, & 0.01 \end{bmatrix}.$$

2. Eight-component Gaussian mixture distribution:

$$\rho(\mathbf{x}) = \frac{1}{8} \sum_{i=1}^8 N(\mathbf{x}|\boldsymbol{\mu}_i, \boldsymbol{\Sigma}),$$

where $\boldsymbol{\mu}_1 = (0, 4)$, $\boldsymbol{\mu}_2 = (2.8, 2.8)$, $\boldsymbol{\mu}_3 = (4, 0)$, $\boldsymbol{\mu}_4 = (-2.8, 2.8)$, $\boldsymbol{\mu}_5 = (-4, 0)$, $\boldsymbol{\mu}_6 = (-2.8, -2.8)$, $\boldsymbol{\mu}_7 = (0, -4)$, $\boldsymbol{\mu}_8 = (2.8, -2.8)$, and $\boldsymbol{\Sigma} = \begin{bmatrix} 0.2, & 0 \\ 0, & 0.2 \end{bmatrix}$.

3. Wave-shaped distribution:

$$\rho(\mathbf{x}) = 9.93^{-1} \exp(-0.1x_1^2 - (x_2 - \sin(\pi x_1))^2).$$

Although the first two distributions are both Gaussian mixture distributions, the eight-component Gaussian mixture distribution is more challenging since the effective support region for each Gaussian component is not connected, unlike the star-shaped distribution.

For all three examples, we set $N = 200$ and `maxIter`=1000, with initial distributions of Uniform $[-2, 2]$, Uniform $[-4, 4]$, and Uniform $[-3, 3]$, respectively. Figure 2 displays the particles at the 100th, 500th, and 1000th iterations across three rows of sub-figures. By the 100th iteration, most particles have moved toward the high-density regions. At the 500th iteration, the particles are largely aligned, with only a few outliers remaining. By the 1000th iteration, even these outliers have converged to the target distribution. This behavior exemplifies the exploration-exploitation trade-off of the EVI-MMD method. In the early stages, a larger bandwidth encourages exploration, guiding particles toward high-density areas. In later stages, a smaller bandwidth facilitates exploitation, refining the alignment of particles to the target distribution.

We compare the proposed Algorithm 2 with other similar methods, including the EVI-Im by Wang et al. (2021), SVGD by Liu (2017), and Langevin Monte Carlo (LMC) by Rossky et al. (1978). For the EVI-Im and SVGD methods, we set the step size $\eta_0 = 0.1$ and a fixed bandwidth $h = 0.1$ for the Gaussian kernel. The tuning parameters of LMC are $a = 0.1$, $b = 1$, and $c = 0.55$, which decides the step size of LMC by the equation $\eta_0 = a(b + n)^{-c}$ (different from the proposed algorithm).

To fairly compare the four algorithms, we compute the MMD² criterion using a fixed bandwidth $h = 0.5$. [What is sample used to compute this MMD.....] So this MMD² is *not* the objective function of any algorithms in this comparison. Figure 3 shows the decreasing MMD² with respect to iterations of all the algorithms. From Figure 3 we can see that the EVI-MMD has the best performance for all three examples.

4.2 Gaussian Distribution with Increasing Dimension

In this example, we study the performance of the proposed algorithm with respect to the increasing dimension. We compare the EVI-MMD with the adaptive bandwidth for the Gaussian kernel with two alternative methods:

- EVI-Energy-Distance: this method means that we set the free energy in Algorithm 1 to be the energy distance in (3) proposed in Székely and Rizzo (2013), i.e., $\mathcal{F}(\{\mathbf{x}_i\}_{i=1}^n) = E(F_n, F)$.
- Support-Points: this method is proposed by Mak and Joseph (2018), which minimizes the same energy distance by a combination of the convex-concave procedure (CCP) with the resampling method.

The EVI-Energy-Distance method and the Support-Points method both minimize the same objective function but use different minimization methods. The EVI-MMD method and the EVI-Energy-Distance method minimize different objective functions but use the same implicit method.

We sample training data of size $M = 50,000$ from a standard Gaussian distribution with dimensions $d = 10, 20, \dots, 100$. The same training data is used to compare the three methods. The same training data is used to compare the three methods, along with identical particle sizes $N = 500$ and initial samples generated from $\text{Uniform}[-2, 2]^d$. For the EVI-MMD method, the tuning parameters (a, b, c) are set as described at the beginning of this section. Both EVI-MMD and EVI-Energy-Distance use `maxIter` = 500 for lower-dimensional examples ($d \leq 60$) and `maxIter` = 5000 for higher-dimensional examples, with a mini-batch size of $L = 5000$. For Support-Points, we adopt the default settings recommended by [Mak and Joseph \(2018\)](#). Figure 4 compares the MMD^2 (using a Gaussian kernel with fixed bandwidth) and the energy distance $E(F_n, F)$ defined in (3) for the particles returned by the three methods after convergence, across dimensions $d = 10, \dots, 100$. Notably, the MMD with a Gaussian kernel can fail if the bandwidth is unsuitable. A reasonable choice is $h = \sqrt{d/2}$, and we fix $h = 5$ for our experiments.

From the 4, we observe that the EVI-MMD method generally outperforms the Support-Points method, except in the $d = 90$ and $d = 100$ cases. Note that the y -axis is in log scale, so the differences between the methods are not substantial. This suggests that EVI-MMD delivers results comparable to those of Support-Points. However, in Section 4.3, the advantage of EVI-MMD becomes much more pronounced, as Support-Points fails to converge, highlighting the robustness and effectiveness of our proposed method.

4.3 Generative Model

Generative learning models have been widely used in various machine learning applications. They can solve supervised and unsupervised learning problems. Simply put, the generative learning model generates new samples based on the training data. More advanced generative learning models are combined with deep neural networks ([Jabbar et al., 2021](#)), Naive Bayes, Gaussian mixture model, hidden Markov model, etc. ([GM et al., 2020](#)). In this example, we use the simplest nonparametric generative learning setup and apply the EVI-MMD to three benchmark image datasets, MNIST ([Lecun et al., 1998](#)), Fashion-MNIST ([Xiao et al., 2017](#)), and Cifar10 ([Krizhevsky and Hinton, 2009](#)).

For the MNIST and Fashion-MNIST datasets, each data point is a grey image of $d = 28 \times 28 = 784$ size of pixels. For the Cifar10 dataset, each data point is a full-color image of $d = 32 \times 32 \times 3 = 3072$ size of pixels. One pixel value is in $[0, 1]$. All three are extremely high-dimensional two-sample problems. For the MNIST and Fashion-MNIST datasets, we use the whole dataset of size $M = 60,000$ as the training data and resample a mini-batch of $L = 100$ samples in each iteration. However, for the Cifar10 dataset, due to the extremely high dimension, we randomly choose a subset of $M = 5000$ images as the training data and also use the mini-batch of the size of $L = 100$. We choose $L = 100$, which is relatively small considering the dimension, is mainly due to the limited computing resources, but it has been proved to be sufficient.

We generate $N = 100$ new images using the EVI-MMD method and the EVI-Energy-Distance method defined in Section 4.2¹. The initial particles are sampled from a uniform distribution in $[0, 1]^d$. We terminate both algorithms at `maxIter` = 500 for the EVI-MMD method. Figure 5 compares side-by-side 100 training data randomly chosen from the original training data (left column), new images generated by EVI-MMD (middle column), and EVI-Energy-Distance (right

¹We do not include the Support-Points method in this comparison because some issues with the R codes by [Mak and Joseph \(2018\)](#). We are not sure the reason but the returned results do not show any sign of convergence.

column). Both the training and new images are put into a 10×10 panel. We can see the new images generated by both methods are very similar to the training data, and the EVI-MMD returns slightly sharper images than the EVI-Energy-Distance method.

To provide a numerical comparison of the two methods, we calculate the FID score (Heusel et al., 2017) of the generated images. Due to the high computational cost, we randomly sample a subset of 500 images from the training data and calculate the FID score between the new images and the subset of training images. Repeating this 10 times we obtain 10 FID scores for each example. Figure 6 shows the boxplots of all the FID scores for the two methods for all three examples. We can see that both methods have a comparable FID score and the EVI-MMD outperforms the EVI-Energy-Distance in the MNIST and Cifar10 examples, which is consistent with the visual comparison in Figure 5.

We also provide the trajectory of the EVI-MMD method in Figure 7. It shows the evolution of some randomly picked particles from static images to the final sharp images. Interestingly, some images are switched directions in the middle of their trajectories. For example, in the second row of the middle panel, the image suddenly switched from a top to a dress then to a pair of pants. This is because when we resample a mini-batch in each iteration. New images can appear in the mini-batch while some old images are not selected, causing the particles to constantly change to approximate the mini-batch data. Note that the EVI-MMD is by no means the best approach for the MNIST benchmark example. Readers can find many more sophisticated generative learning approaches that return better results. However, the EVI-MMD is probably the simplest by comparison and its results are adequate.

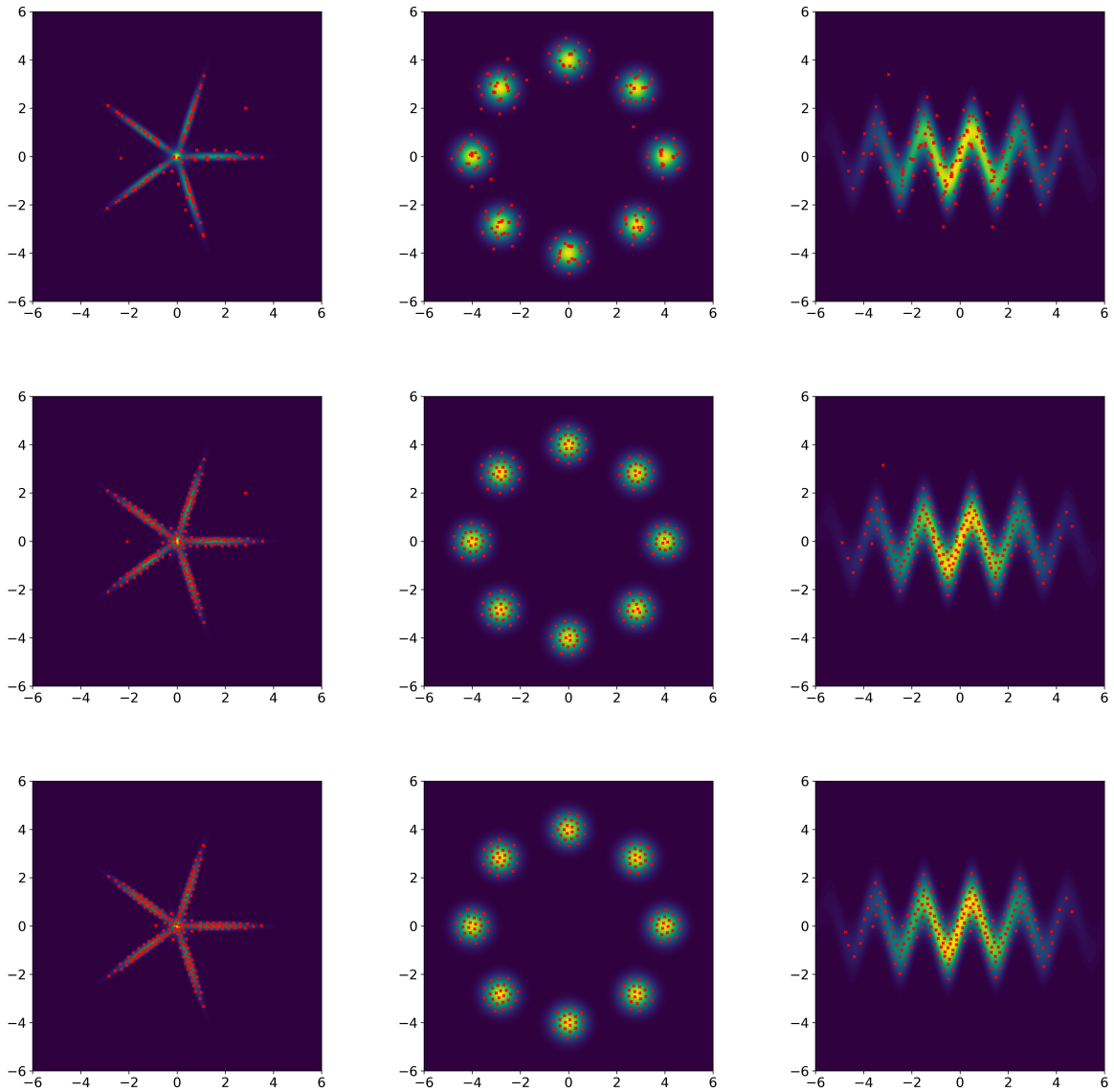


Figure 2: From top to bottom, each column of sub-figures show the particles by the EVI-MMD algorithm at $n = 100$, $n = 500$, and $n = 1000$ iterations. The target density function is plotted as the contour in the background.

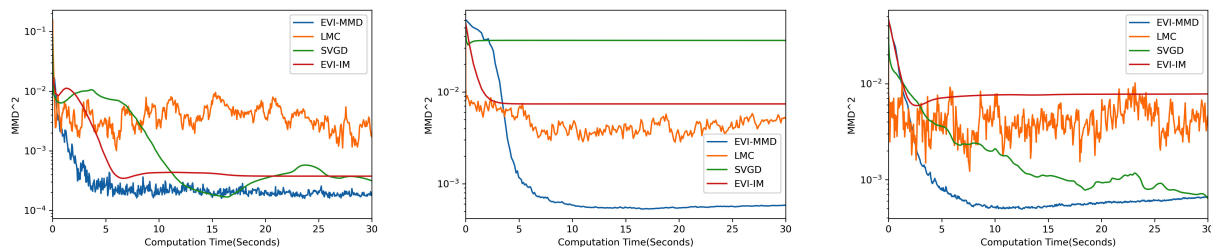


Figure 3: From left to right, the three sub-figures show the decreasing MMD^2 of four methods for the three toy examples with the target distributions star-shaped five-component Gaussian mixture distribution, eight-component Gaussian mixture distribution, and wave-shaped distribution.

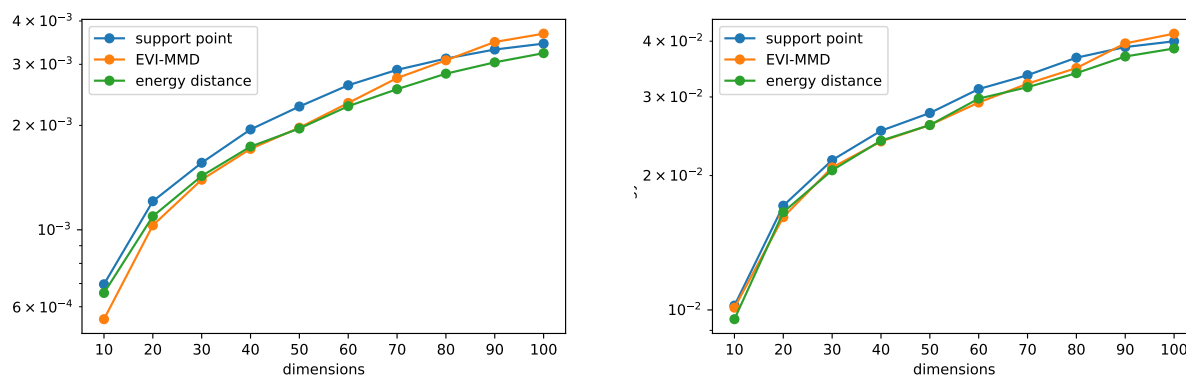


Figure 4: The MMD^2 criterion (Gaussian kernel with $h = 5$) (left) and energy distance criterion (right) of the particles returned by three methods: blue curve for Support-Point, orange curve for EVI-MMD, and green curve for EVI-Energy Distance.

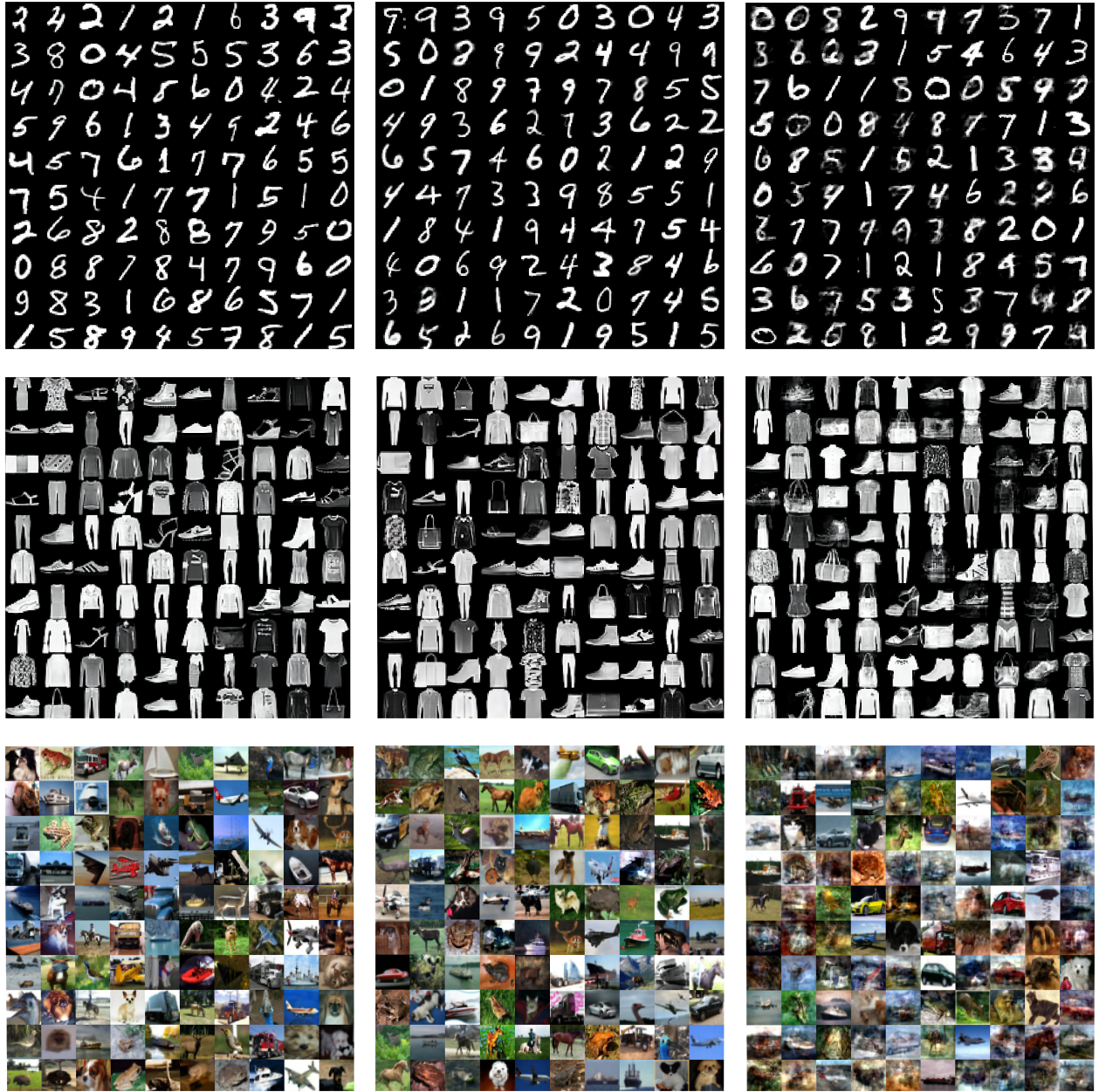


Figure 5: Visual comparison between 100 training data randomly chosen from the original training data (left column), new images generated by EVI-MMD (middle column), and EVI-Energy-Distance (right column).

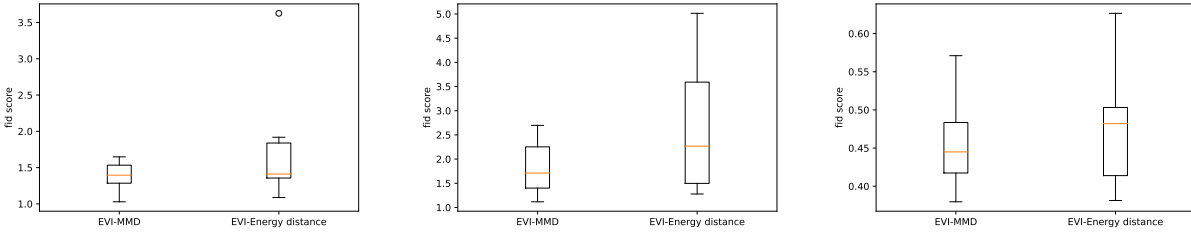


Figure 6: Boxplot of FID scores for the examples, MNIST, MNIST-Fashion and CIFAR10 returned by EVI-MMD (left box) and EVI-Energy-Distance (right box).

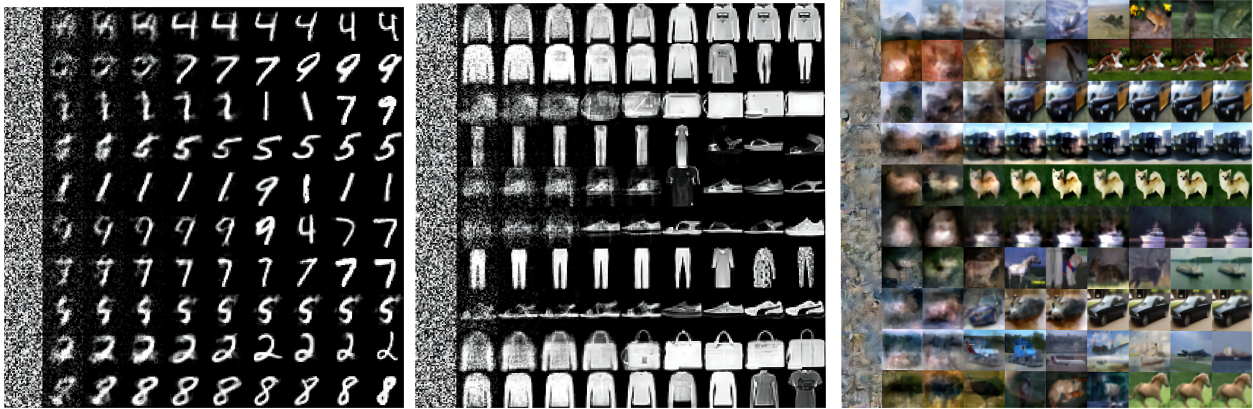


Figure 7: The trajectories of the movement of some randomly picked particles of the EVI-MMD method.

5 Conclusion

In this paper, we develop a new deterministic sampling method to approximate a target distribution by minimizing the kernel discrepancy, alternatively known as maximum mean discrepancy (MMD). The minimization of MMD is solved by the general energetic variational inference (EVI) framework first introduced by Wang et al. (2021). Specifically, we use the quadratic dissipation functional of the EVI and apply the particle approximation to the continuous energy-dissipation law, which is then followed by the variation procedure. This leads to a dynamic system that moves the particles from their initial positions to the target distribution. Using the implicit Euler scheme to solve this dynamic system, we obtain a special algorithm based on the EVI framework to minimize MMD, which we call EVI-MMD algorithm. In each iteration of updating the particles, we solve a proximal minimization problem using algorithms such as L-BFGS. To overcome the long-existing issue of bandwidth selection of the Gaussian kernel, we propose a novel way to specify the bandwidth dynamically. Other than approximating a fully specified distribution that is difficult to sample from, the EVI-MMD algorithm can also be used as a generative learning model for two-sample problems.

The EVI framework is very general. Many new variational inference methods can be proposed if we choose different combinations of the key components of the EVI framework. Such key components include the choice of divergence functionals, order of variational and discretization of the continuous EVI scheme, using parametric or non-parametric model for the flow map, and various numerical schemes for solving the dynamic system, etc. In fact, some existing methods can be also included in the EVI framework. The unified EVI framework also paves the way for a unified theoretical foundation for similar algorithms. We will keep pursuing these directions and fully explore the potentials of the EVI framework.

Acknowledgment

This research was done using services provided by the OSG Consortium (Pordes et al., 2007; Sfligoi et al., 2009), which is supported by the National Science Foundation awards # 2030508 and # 1836650. We thank the editor, associate editor, and two reviewers for their valuable comments and suggestions. L. Kang’s work is partially supported by the National Science Foundation Grants DMS-1916467 and DMS-2153029. Y. Wang and C. Liu are partially supported by the National Science Foundation Grant DMS-1759536, DMS-1950868, and DMS-2153029.

References

- Arbel, M., Korba, A., SALIM, A., and Gretton, A. (2019), “Maximum Mean Discrepancy Gradient Flow,” in *Advances in Neural Information Processing Systems*, eds. Wallach, H., Larochelle, H., Beygelzimer, A., d’Alché-Buc, F., Fox, E., and Garnett, R., Curran Associates, Inc., vol. 32.
- Bernton, E. (2018), “Langevin Monte Carlo and JKO splitting,” in *Proceedings of the 31st Conference On Learning Theory*, eds. Bubeck, S., Perchet, V., and Rigollet, P., PMLR, vol. 75 of *Proceedings of Machine Learning Research*, pp. 1777–1798.
- Bińkowski, M., Sutherland, D. J., Arbel, M., and Gretton, A. (2021), “Demystifying MMD GANs,” *arXiv preprint arXiv:1806.06317*.
- Briol, F.-X., Barp, A., Duncan, A. B., and Girolami, M. (2019), “Statistical Inference for Generative Models with Maximum Mean Discrepancy,” *arXiv preprint arXiv:1906.05944*.

- Chen, C., Zhang, R., Wang, W., Li, B., and Chen, L. (2018a), “A unified particle-optimization framework for scalable bayesian sampling,” *arXiv preprint arXiv:1805.11659*.
- Chen, P., Wu, K., Chen, J., O’Leary-Roseberry, T., and Ghattas, O. (2019a), “Projected Stein Variational Newton: A Fast and Scalable Bayesian Inference Method in High Dimensions,” in *Advances in Neural Information Processing Systems*, eds. Wallach, H., Larochelle, H., Beygelzimer, A., d’Alché-Buc, F., Fox, E., and Garnett, R., Curran Associates, Inc., vol. 32, pp. 5184–5194.
- (2019b), “Projected Stein Variational Newton: A Fast and Scalable Bayesian Inference Method in High Dimensions,” in *Advances in Neural Information Processing Systems*, eds. Wallach, H., Larochelle, H., Beygelzimer, A., d’Alché-Buc, F., Fox, E., and Garnett, R., Curran Associates, Inc., vol. 32, pp. 15130–15139.
- (2019c), “Projected Stein Variational Newton: A Fast and Scalable Bayesian Inference Method in High Dimensions,” in *Advances in Neural Information Processing Systems*, eds. Wallach, H., Larochelle, H., Beygelzimer, A., d’Alché-Buc, F., Fox, E., and Garnett, R., Curran Associates, Inc., vol. 32.
- Chen, W. Y., Mackey, L., Gorham, J., Briol, F.-X., and Oates, C. (2018b), “Stein Points,” in *Proceedings of the 35th International Conference on Machine Learning*, eds. Dy, J. and Krause, A., PMLR, vol. 80 of *Proceedings of Machine Learning Research*, pp. 844–853.
- Cheng, X., Chatterji, N. S., Bartlett, P. L., and Jordan, M. I. (2018), “Underdamped Langevin MCMC: A non-asymptotic analysis,” in *Proceedings of the 31st Conference On Learning Theory*, eds. Bubeck, S., Perchet, V., and Rigollet, P., PMLR, vol. 75 of *Proceedings of Machine Learning Research*, pp. 300–323.
- Creswell, A., White, T., Dumoulin, V., Arulkumaran, K., Sengupta, B., and Bharath, A. A. (2018), “Generative Adversarial Networks: An Overview,” *IEEE Signal Processing Magazine*, 35, 53–65.
- Csiszár, I. and Shields, P. (2004), “Information Theory and Statistics: A Tutorial,” *Foundations and Trends in Communications and Information Theory*, 1, 417–528.
- Damianou, A. C., Titsias, M. K., and Lawrence, N. D. (2016), “Variational inference for latent variables and uncertain inputs in Gaussian processes,” *The Journal of Machine Learning Research*, 17, 1425–1486.
- David M. Blei, A. K. and McAuliffe, J. D. (2017), “Variational Inference: A Review for Statisticians,” *Journal of the American Statistical Association*, 112, 859–877.
- E, W., Ma, C., and Wu, L. (2020), “Machine learning from a continuous viewpoint, I,” *Science China Mathematics*, 63, 2233–2266.
- Fang, K.-T., Lin, D. K., Winker, P., and Zhang, Y. (2000), “Uniform design: theory and application,” *Technometrics*, 42, 237–248.
- Fang, K.-T., Ma, C.-X., and Winker, P. (2002), “Centered L_2 -discrepancy of random sampling and Latin hypercube design, and construction of uniform designs,” *Mathematics of Computation*, 71, 275–296.
- Fang, K.-T. and Mukerjee, R. (2000), “Miscellanea. A connection between uniformity and aberration in regular fractions of two-level factorials,” *Biometrika*, 87, 193–198.

- Fukumizu, K., Gretton, A., Sun, X., and Schölkopf, B. (2007), “Kernel Measures of Conditional Dependence,” in *Advances in Neural Information Processing Systems*, eds. Platt, J., Koller, D., Singer, Y., and Roweis, S., Curran Associates, Inc., vol. 20, pp. 489–496.
- Giga, M.-H., Kirshtein, A., and Liu, C. (2017), “Variational Modeling and Complex Fluids,” in *Handbook of Mathematical Analysis in Mechanics of Viscous Fluids*, eds. Giga, Y. and Novotny, A., Springer International Publishing, pp. 1–41.
- GM, H., Gourisaria, M. K., Pandey, M., and Rautaray, S. S. (2020), “A comprehensive survey and analysis of generative models in machine learning,” *Computer Science Review*, 38, 100285.
- Goodfellow, I., Pouget-Abadie, J., Mirza, M., Xu, B., Warde-Farley, D., Ozair, S., Courville, A., and Bengio, Y. (2014), “Generative Adversarial Nets,” in *Advances in Neural Information Processing Systems*, eds. Ghahramani, Z., Welling, M., Cortes, C., Lawrence, N., and Weinberger, K., Curran Associates, Inc., vol. 27.
- Gorbach, N. S., Bauer, S., and Buhmann, J. M. (2017), “Scalable Variational Inference for Dynamical Systems,” in *Advances in Neural Information Processing Systems*, eds. Guyon, I., Luxburg, U. V., Bengio, S., Wallach, H., Fergus, R., Vishwanathan, S., and Garnett, R., Curran Associates, Inc., vol. 30, pp. 4807–4816.
- Graves, A. (2011), “Practical Variational Inference for Neural Networks,” in *Advances in Neural Information Processing Systems*, eds. Shawe-Taylor, J., Zemel, R., Bartlett, P., Pereira, F., and Weinberger, K., Curran Associates, Inc., vol. 24, pp. 2348–2356.
- Gretton, A., Borgwardt, K. M., Rasch, M. J., Schölkopf, B., and Smola, A. (2012), “A kernel two-sample test,” *The Journal of Machine Learning Research*, 13, 723–773.
- Heng, J., Doucet, A., and Pokern, Y. (2021), “Gibbs Flow for Approximate Transport with Applications to Bayesian Computation,” *Journal of the Royal Statistical Society Series B: Statistical Methodology*, 83, 156–187.
- Heusel, M., Ramsauer, H., Unterthiner, T., Nessler, B., and Hochreiter, S. (2017), “GANs Trained by a Two Time-Scale Update Rule Converge to a Local Nash Equilibrium,” in *Advances in Neural Information Processing Systems*, eds. Guyon, I., Luxburg, U. V., Bengio, S., Wallach, H., Fergus, R., Vishwanathan, S., and Garnett, R., Curran Associates, Inc., vol. 30.
- Hickernell, F. (1998), “A generalized discrepancy and quadrature error bound,” *Mathematics of computation*, 67, 299–322.
- Hickernell, F. J. (1999), “Goodness-of-fit statistics, discrepancies and robust designs,” *Statistics & probability letters*, 44, 73–78.
- (2016), “The trio identity for Quasi-Monte Carlo error,” in *International Conference on Monte Carlo and Quasi-Monte Carlo Methods in Scientific Computing*, Springer, pp. 3–27.
- Hickernell, F. J. and Liu, M.-Q. (2002), “Uniform designs limit aliasing,” *Biometrika*, 89, 893–904.
- Jabbar, A., Li, X., and Omar, B. (2021), “A Survey on Generative Adversarial Networks: Variants, Applications, and Training,” *ACM Computing Surveys (CSUR)*, 54.
- Jordan, M. I., Ghahramani, Z., Jaakkola, T. S., and Saul, L. K. (1999), “An Introduction to Variational Methods for Graphical Models,” *Machine Learning*, 37, 183–233.

- Jordan, R., Kinderlehrer, D., and Otto, F. (1998), “The variational formulation of the Fokker–Planck equation,” *SIAM journal on mathematical analysis*, 29, 1–17.
- King, N. J. and Lawrence, N. D. (2006), “Fast Variational Inference for Gaussian Process Models Through KL-Correction,” in *Machine Learning: ECML 2006*, eds. Fürnkranz, J., Scheffer, T., and Spiliopoulou, M., Berlin, Heidelberg: Springer Berlin Heidelberg, pp. 270–281.
- Kingma, D. P., Mohamed, S., Jimenez Rezende, D., and Welling, M. (2014), “Semi-supervised Learning with Deep Generative Models,” in *Advances in Neural Information Processing Systems*, eds. Ghahramani, Z., Welling, M., Cortes, C., Lawrence, N., and Weinberger, K., Curran Associates, Inc., vol. 27, pp. 3581–3589.
- Kingma, D. P., Salimans, T., Jozefowicz, R., Chen, X., Sutskever, I., and Welling, M. (2016a), “Improved Variational Inference with Inverse Autoregressive Flow,” in *Advances in Neural Information Processing Systems*, eds. Lee, D., Sugiyama, M., Luxburg, U., Guyon, I., and Garnett, R., Curran Associates, Inc., vol. 29, pp. 2200–2210.
- (2016b), “Improved Variational Inference with Inverse Autoregressive Flow,” in *Advances in Neural Information Processing Systems*, eds. Lee, D., Sugiyama, M., Luxburg, U., Guyon, I., and Garnett, R., Curran Associates, Inc., vol. 29, pp. 4743–4751.
- Kingma, D. P. and Welling, M. (2013), “Auto-encoding variational bayes,” *arXiv preprint arXiv:1312.6114*.
- Korba, A., Aubin-Frankowski, P.-C., Majewski, S., and Ablin, P. (2021), “Kernel Stein Discrepancy Descent,” in *Proceedings of the 38th International Conference on Machine Learning*, eds. Meila, M. and Zhang, T., PMLR, vol. 139 of *Proceedings of Machine Learning Research*, pp. 5719–5730.
- Krizhevsky, A. and Hinton, G. (2009), “Learning multiple layers of features from tiny images,” Tech. Rep. 0, University of Toronto, Toronto, Ontario.
- Lecun, Y., Bottou, L., Bengio, Y., and Haffner, P. (1998), “Gradient-based learning applied to document recognition,” *Proceedings of the IEEE*, 86, 2278–2324.
- Li, Y., Kang, L., and Hickernell, F. J. (2020), “Is a Transformed Low Discrepancy Design Also Low Discrepancy?” in *Contemporary Experimental Design, Multivariate Analysis and Data Mining*, Springer, pp. 69–92.
- Li, Y., Swersky, K., and Zemel, R. (2015), “Generative Moment Matching Networks,” in *Proceedings of the 32nd International Conference on Machine Learning*, eds. Bach, F. and Blei, D., Lille, France: PMLR, vol. 37 of *Proceedings of Machine Learning Research*, pp. 1718–1727.
- Liu, C. and Zhu, J. (2018), “Riemannian Stein Variational Gradient Descent for Bayesian Inference,” *Proceedings of the AAAI Conference on Artificial Intelligence*, 32.
- Liu, C., Zhuo, J., Cheng, P., Zhang, R., and Zhu, J. (2019), “Understanding and Accelerating Particle-Based Variational Inference,” in *Proceedings of the 36th International Conference on Machine Learning*, eds. Chaudhuri, K. and Salakhutdinov, R., PMLR, vol. 97 of *Proceedings of Machine Learning Research*, pp. 4082–4092.
- Liu, D. C. and Nocedal, J. (1989), “On the limited memory BFGS method for large scale optimization,” *Mathematical Programming*, 45, 503–528.

- Liu, Q. (2017), “Stein Variational Gradient Descent as Gradient Flow,” in *Advances in Neural Information Processing Systems*, eds. Guyon, I., Luxburg, U. V., Bengio, S., Wallach, H., Fergus, R., Vishwanathan, S., and Garnett, R., Curran Associates, Inc., vol. 30, pp. 3115–3123.
- Liu, Q., Lee, J., and Jordan, M. (2016), “A Kernelized Stein Discrepancy for Goodness-of-fit Tests,” in *Proceedings of The 33rd International Conference on Machine Learning*, eds. Balcan, M. F. and Weinberger, K. Q., New York, New York, USA: PMLR, vol. 48 of *Proceedings of Machine Learning Research*, pp. 276–284.
- Liu, Q. and Wang, D. (2016), “Stein Variational Gradient Descent: A General Purpose Bayesian Inference Algorithm,” in *Advances in Neural Information Processing Systems*, eds. Lee, D., Sugiyama, M., Luxburg, U., Guyon, I., and Garnett, R., Curran Associates, Inc., vol. 29, pp. 2378–2386.
- Louizos, C. and Welling, M. (2017), “Multiplicative Normalizing Flows for Variational Bayesian Neural Networks,” in *Proceedings of the 34th International Conference on Machine Learning - Volume 70*, JMLR.org, ICML’17, p. 2218–2227.
- Ma, Y.-A., Chen, Y., Jin, C., Flammarion, N., and Jordan, M. I. (2019), “Sampling can be faster than optimization,” *Proceedings of the National Academy of Sciences*, 116, 20881–20885.
- Mak, S. and Joseph, V. R. (2018), “Support points,” *The Annals of Statistics*, 46, 2562–2592.
- Marius Hofert, A. P. and Zhu, M. (2021), “Quasi-Random Sampling for Multivariate Distributions via Generative Neural Networks,” *Journal of Computational and Graphical Statistics*, 30, 647–670.
- Micchelli, C. A., Xu, Y., and Zhang, H. (2006), “Universal Kernels.” *The Journal of Machine Learning Research*, 7, 2651–2667.
- Mnih, A. and Rezende, D. (2016), “Variational Inference for Monte Carlo Objectives,” in *Proceedings of The 33rd International Conference on Machine Learning*, eds. Balcan, M. F. and Weinberger, K. Q., New York, New York, USA: PMLR, vol. 48 of *Proceedings of Machine Learning Research*, pp. 2188–2196.
- Mroueh, Y., Sercu, T., and Raj, A. (2019), “Sobolev Descent,” in *Proceedings of the Twenty-Second International Conference on Artificial Intelligence and Statistics*, eds. Chaudhuri, K. and Sugiyama, M., PMLR, vol. 89 of *Proceedings of Machine Learning Research*, pp. 2976–2985.
- Nguyen, T. and Bonilla, E. (2013), “Efficient Variational Inference for Gaussian Process Regression Networks,” in *Proceedings of the Sixteenth International Conference on Artificial Intelligence and Statistics*, eds. Carvalho, C. M. and Ravikumar, P., Scottsdale, Arizona, USA: PMLR, vol. 31 of *Proceedings of Machine Learning Research*, pp. 472–480.
- Nguyen, T. V. and Bonilla, E. V. (2014), “Automated Variational Inference for Gaussian Process Models,” in *Advances in Neural Information Processing Systems 27*, eds. Ghahramani, Z., Welling, M., Cortes, C., Lawrence, N. D., and Weinberger, K. Q., Curran Associates, Inc., pp. 1404–1412.
- Onsager, L. (1931a), “Reciprocal relations in irreversible processes. I.” *Phys. Rev.*, 37, 405.
- (1931b), “Reciprocal relations in irreversible processes. II.” *Phys. Rev.*, 38, 2265.

- Paszke, A., Gross, S., Massa, F., Lerer, A., Bradbury, J., Chanan, G., Killeen, T., Lin, Z., Gimelshein, N., Antiga, L., Desmaison, A., Kopf, A., Yang, E., DeVito, Z., Raison, M., Tejani, A., Chilamkurthy, S., Steiner, B., Fang, L., Bai, J., and Chintala, S. (2019), “PyTorch: An Imperative Style, High-Performance Deep Learning Library,” in *Advances in Neural Information Processing Systems 32*, eds. Wallach, H., Larochelle, H., Beygelzimer, A., d'Alché-Buc, F., Fox, E., and Garnett, R., Curran Associates, Inc., pp. 8024–8035.
- Pordes, R., Petravick, D., Kramer, B., Olson, D., Livny, M., Roy, A., Avery, P., Blackburn, K., Wenaus, T., Würthwein, F., Foster, I., Gardner, R., Wilde, M., Blatecky, A., McGee, J., and Quick, R. (2007), “The open science grid,” in *J. Phys. Conf. Ser.*, vol. 78 of 78, p. 012057.
- Rayleigh, L. (1873), “Some General Theorems Relating to Vibrations,” *Proceedings of the London Mathematical Society*, 4, 357–368.
- Rezende, D. and Mohamed, S. (2015), “Variational Inference with Normalizing Flows,” in *Proceedings of the 32nd International Conference on Machine Learning*, eds. Bach, F. and Blei, D., Lille, France: PMLR, vol. 37 of *Proceedings of Machine Learning Research*, pp. 1530–1538.
- Rockafellar, R. T. (1976), “Monotone operators and the proximal point algorithm,” *SIAM journal on control and optimization*, 14, 877–898.
- Rosky, P. J., Doll, J. D., and Friedman, H. L. (1978), “Brownian dynamics as smart Monte Carlo simulation,” *The Journal of Chemical Physics*, 69, 4628–4633.
- Sfiligoi, I., Bradley, D. C., Holzman, B., Mhashilkar, P., Padhi, S., and Wurthwein, F. (2009), “The pilot way to grid resources using glideinWMS,” in *2009 WRI World Congress on Computer Science and Information Engineering*, vol. 2 of 2, pp. 428–432.
- Sheth, R., Wang, Y., and Kharon, R. (2015), “Sparse Variational Inference for Generalized GP Models,” in *Proceedings of the 32nd International Conference on Machine Learning*, eds. Bach, F. and Blei, D., Lille, France: PMLR, vol. 37 of *Proceedings of Machine Learning Research*, pp. 1302–1311.
- Shridhar, K., Laumann, F., and Liwicki, M. (2019), “A comprehensive guide to bayesian convolutional neural network with variational inference,” *arXiv preprint arXiv:1901.02731*.
- Székel, G. J. and Rizzo, M. L. (2013), “Energy statistics: A class of statistics based on distances,” *Journal of statistical planning and inference*, 143, 1249–1272.
- Trillos, N. G. and Sanz-Alonso, D. (2020), “The Bayesian Update: Variational Formulations and Gradient Flows,” *Bayesian Analysis*, 15, 29 – 56.
- Villani, C. (2021), *Topics in optimal transportation*, vol. 58, American Mathematical Soc.
- Wang, Y., Chen, J., Liu, C., and Kang, L. (2021), “Particle-based energetic variational inference,” *Statistics and Computing*, 31, 1–17.
- Welling, M. and Teh, Y. W. (2011), “Bayesian learning via stochastic gradient langevin dynamics,” in *Proceedings of the 28th International Conference on International Conference on Machine Learning*, Madison, WI, USA: Omnipress, ICML’11, p. 681–688.
- Wibisono, A., Wilson, A. C., and Jordan, M. I. (2016), “A variational perspective on accelerated methods in optimization,” *Proceedings of the National Academy of Sciences*, 113, E7351–E7358.

- Wu, A., Nowozin, S., Meeds, E., Turner, R., Hernández-Lobato, J., and Gaunt, A. (2019), “Deterministic variational inference for robust Bayesian neural networks,” in *7th International Conference on Learning Representations, ICLR 2019*.
- Xiao, H., Rasul, K., and Vollgraf, R. (2017), “Fashion-MNIST: a Novel Image Dataset for Benchmarking Machine Learning Algorithms,” *arXiv:1708.07747*.
- Zhang, M., Bird, T., Habib, R., Xu, T., and Barber, D. (2019), “Variational f-divergence minimization,” *arXiv preprint arXiv:1907.11891*.

Supplement: Tuning The Bandwidth Parameters of the Kernel Function

Choosing the tuning parameters a , c , and τ based on sound theoretical results is challenging. In Section 3.4, we provided a rough rule-of-thumb for their selection. Here, we conduct a more detailed study of these parameters using the eight-component Gaussian mixture distribution.

The first row of Figure S1 (from left to right) shows the distribution of particles at iterations $\text{iter} = 10, 50, 200, 400$ using the same parameters as in Section 4.1. The remaining rows in Figure S1 illustrate the effects of increasing or decreasing the value of c , while keeping other parameters fixed. For each sub-figure, iterations are chosen such that the bandwidth h_n is numerically similar column-wise. The title of each sub-figure indicates the corresponding iterations. Thus, the first row of Figure S1 serves as a reference, while the other rows demonstrate the impact of varying c . Similarly, Figure S2 explores the role of the parameter a .

Two key observations emerge. First, in both Figures S1 and S2, particles in high-density regions exhibit similar alignment for comparable bandwidths h_n . Second, particles initially located in low-density areas tend to remain as outliers even after 200 iterations, reflecting the trade-off between exploration and exploitation.

For the case $c = 0.6$ and $a = 5$, the overall performance aligns with the proposed parameter settings in the toy example (Section 4.1). However, achieving the same bandwidth requires more iterations, as h_n decreases more slowly than in Section 4.1. The exception is the case $a = 2$, where the initial bandwidth is too large, causing some particles to be pushed away and fail to converge before the bandwidth decreases to the exploitation stage. This issue is resolved by using the median trick, as shown in the first row of Figure S2.

Next, we examine the choice of τ . As shown in Figure S3, when τ is too small, particles cannot converge quickly enough before the bandwidth becomes small enough for the exploitation stage. A higher τ yields results similar to the proposed settings in Section 4.1. However, when $\tau = \infty$ (equivalent to solving the problem explicitly), some particles collapse into a single point. This motivates the use of the implicit scheme over the explicit scheme.

In conclusion, the convergence speed primarily depends on the bandwidth h_n . Selecting a , c , and τ involves balancing exploration (moving particles to high-density regions) and exploitation (local refinement). If outliers are prevalent, a slightly smaller c or a larger initial bandwidth $h_0 = a$ is recommended. To accelerate convergence for most particles, increasing c or reducing the initial bandwidth $h_0 = a$ can be effective.

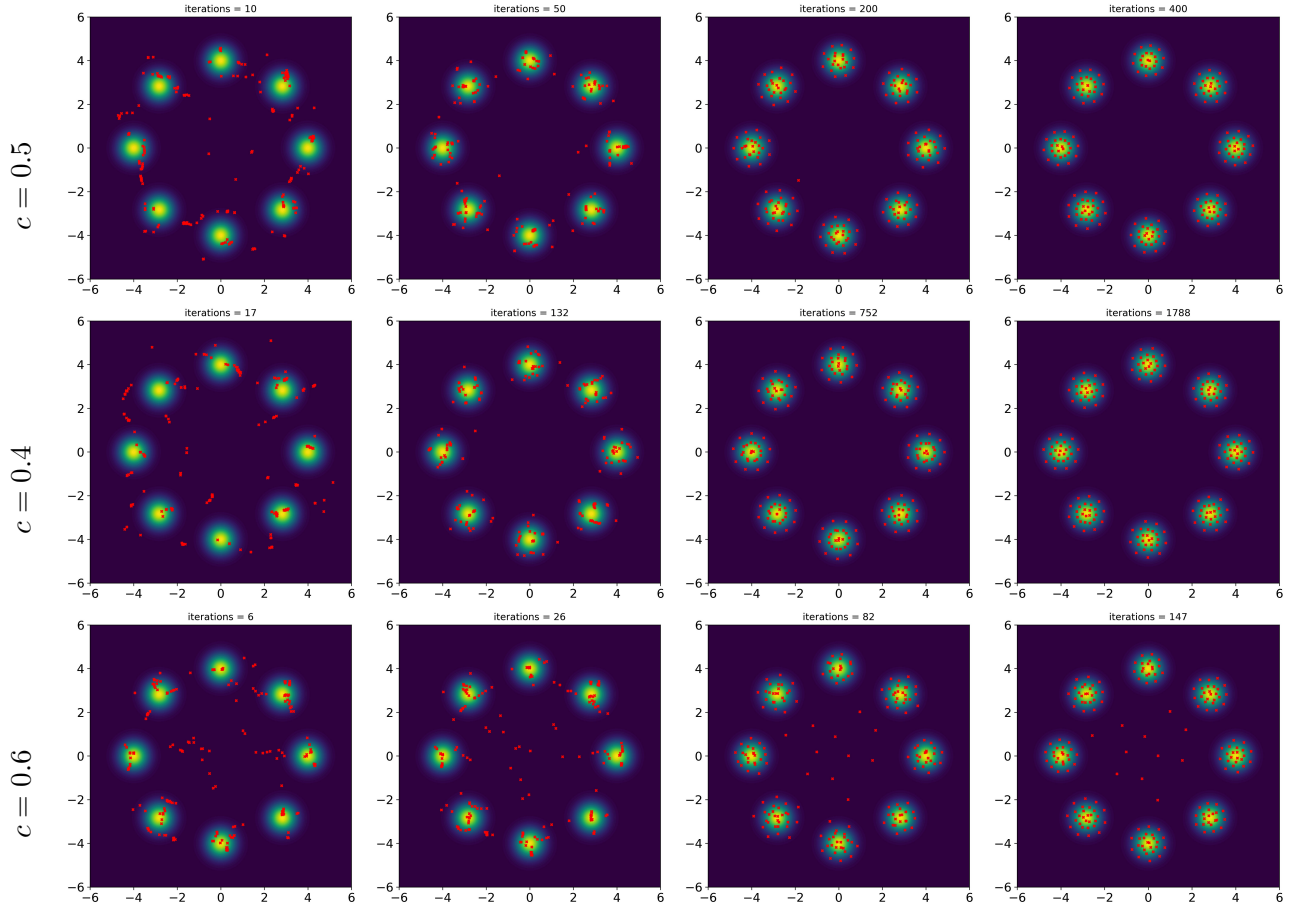


Figure S1: Particle trajectories of different choice of c . In the first row, $c = 0.5$ as in the toy example; in the second row: $c = 0.4$; in the third row: $c = 0.6$. For each figure of the same column, the value of h_n is similar.

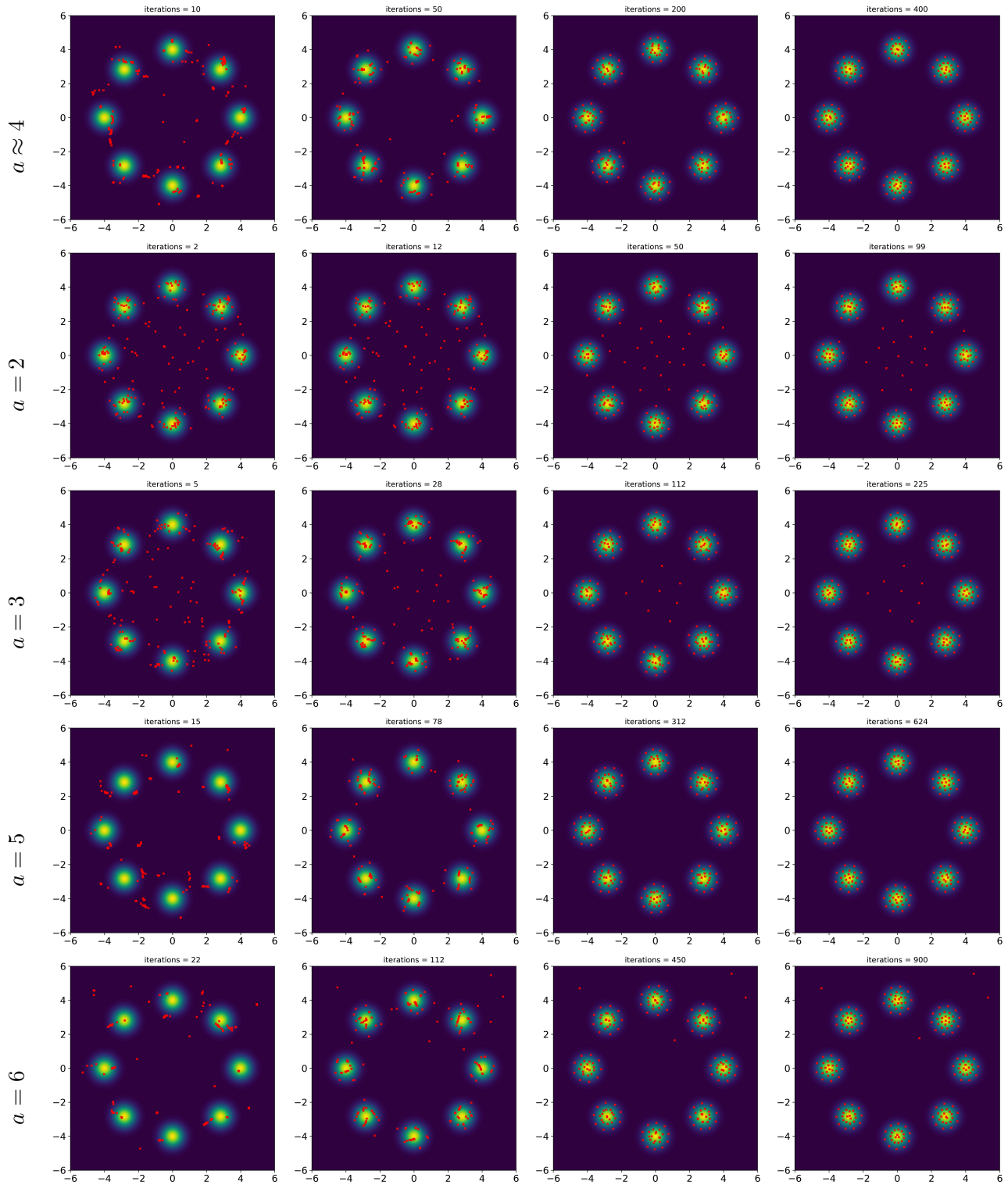


Figure S2: Particle trajectories of different choice of a . In the first row, $a \approx 4$, the median of the pairwise distance of the initial particles as in the toy example; in the remaining rows, $a = 2, 3$, and 5 , respectively. For each sub-figure of the same column, the value of h_n is similar.

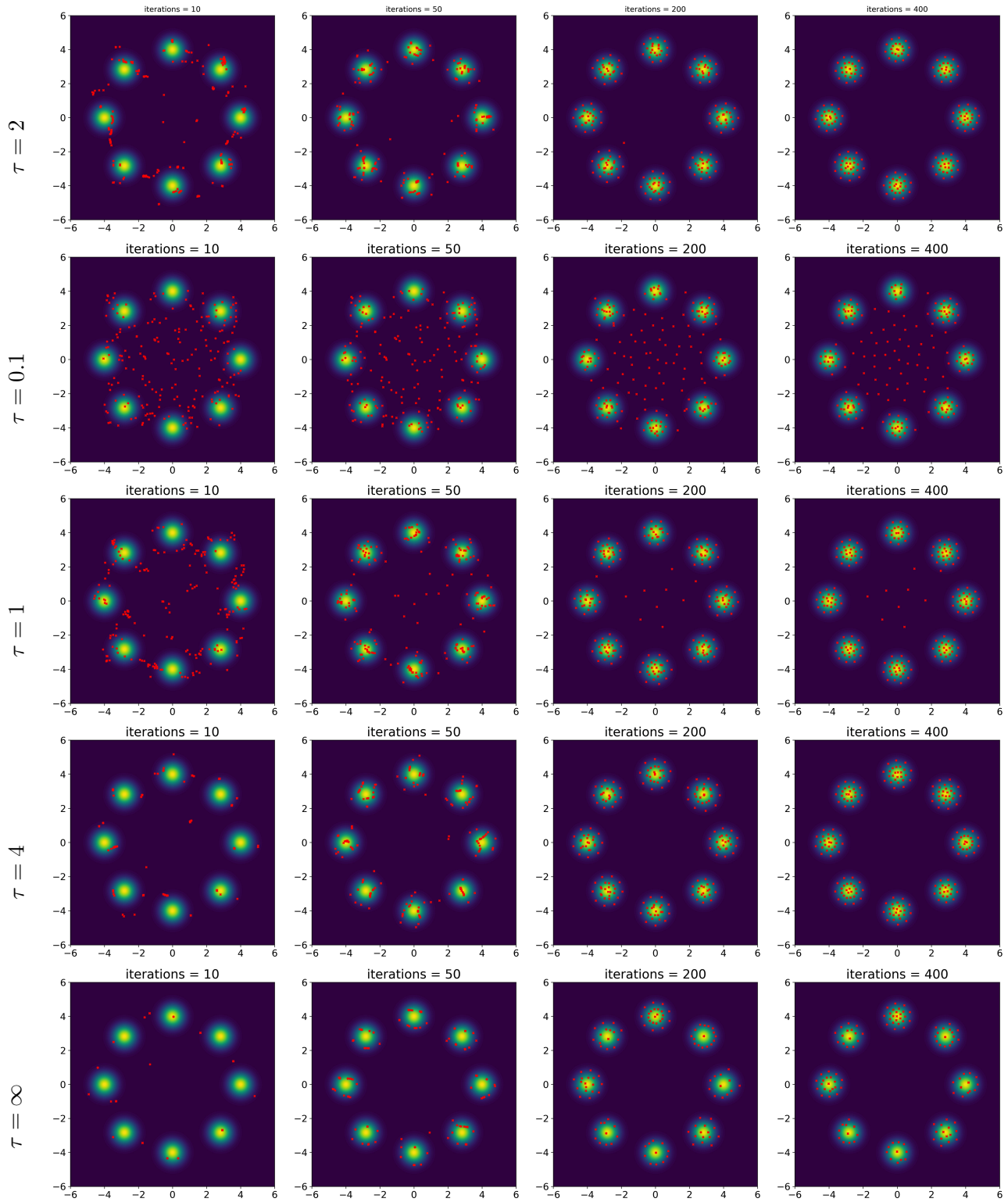


Figure S3: Particle trajectories of different choice of τ . In the first row, $\tau = 2$ as in the toy example; in the remaining rows, $\tau = 0.1, 1, 4$ and ∞ , respectively. For each sub-figure of the same column, the value of h_n is similar.